Supplementary Information (ESI) for the paper

Low pH constructed Co(II) and Ni(II) 1D coordination polymers based on C_α-substituted analogues of zoledronic acid: Structural characterization, spectroscopic and magnetic properties

Tomasz Rojek[a], Waldemar Goldeman[a], Katarzyna Ślepokura[b], Marek Duczmal[a], Agnieszka Wojciechowska[a], Ewa Matczak-Jon[a*]

[a]Department of Chemistry, Wrocław University of Science and Technology, Wybrzeże Wyspiańskiego 27, 50-370 Wrocław, Poland. E-mail: ewa.matczak-jon@pwr.edu.pl

[b]Faculty of Chemistry, University of Wrocław, Joliot-Curie 14, 50-383 Wrocław, Poland.

Table S1. Coordination modes of BPs in known 1D metal complexes of 1:1 molar ratio with various metal ions.

Lp.	*Database refcode*	*Formula*[a]	*Space group*	*Coordination mode*	*Source*
Coordination mode Ia					
1.	LILQII	$[Ca(H_2Ale)]\cdot H_2O$	$P2_12_12_1$	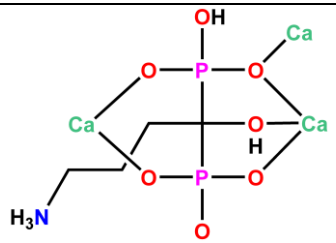	E. Alvarez *et al.*, *CrystEngComm*, **15** (2013) 9899-9905
2.	ODEPEV	$[Cd(H_24py\text{-}Ris)]\cdot H_2O$	$P2_1/c$	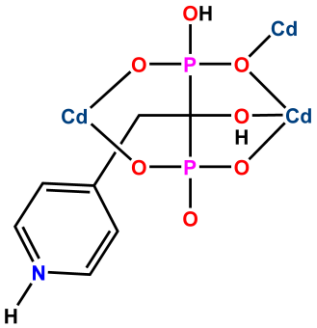	W.-Y. Yin *et al.*, *J. Mol. Eng. Mater.*, **2** (2014) 1440003
3.	YUDPAP	$[Mn(H_2Ris)]\cdot 3H_2O$	$P\bar{1}$	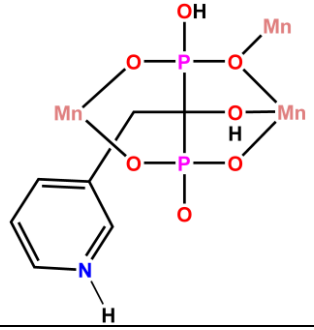	Y. Ma *et al.*, *Inorg. Chem. Commun.*, **12** (2009) 860-863

Coordination mode Ib					
1.	GIKPEW	$[Mn(H_2Ale)]\cdot H_2O$	$P2_1/c$	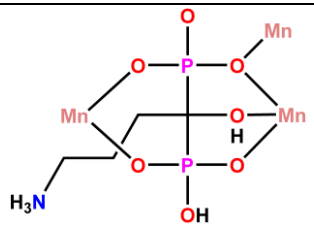	Z.-C. Zhang *et al.*, *Inorg. Chem. Commun.*, **10** (2007) 1063-1066
2.	XEHTAG	$[Mn(H_2Pam)]\cdot H_2O$	$P\bar{1}$	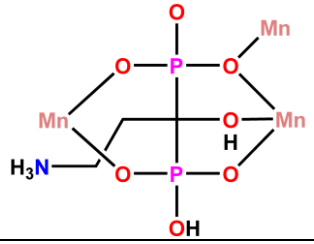	Y. Gong *et al.*, *Inorg. Chem.*, **45** (2006) 4987-4995
Coordination mode Ic					
1.	XEHTEK	$[Co(H_2Pam)]\cdot H_2O$	$P\bar{1}$	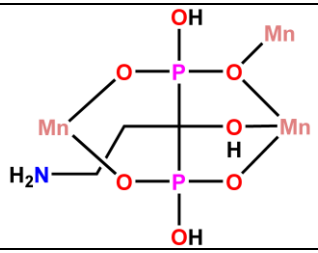	Y. Gong *et al.*, *Inorg. Chem.*, **45** (2006) 4987-4995
Coordination mode IIa					
1.	GAPSIC	$[Cd(H_2Ris)]\cdot H_2O$	$P2_1/c$	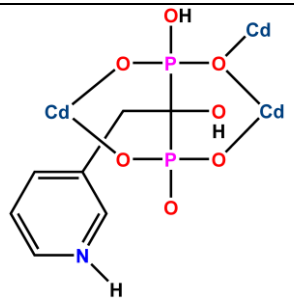	K.-R. Ma *et al.*, *J. Mol. Struct.*, **1139** (2017) 67-77

2.	ODEPAR	[Zn($H_2$4py-Ris)]·H_2O	$P2_1/c$	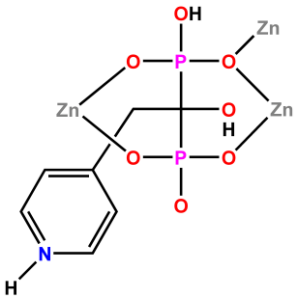	W.-Y. Yin *et al.*, *J. Mol. Eng. Mater.*, **2** (2014) 1440003
3.	OGASOG	[Mn($H_2$4py-Ris)]·H_2O	$P2_1/c$	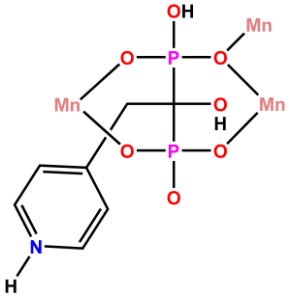	Y.-S. Ma *et al.*, *RSC Adv.*, **3** (2013) 18430-18440
4.	OGATUN	[Co($H_2$4py-Ris)]·H_2O	$P2_1/c$	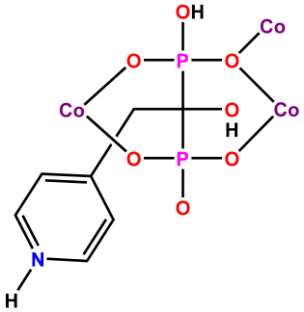	Y.-S. Ma *et al.*, *RSC Adv.*, **3** (2013) 18430-18440

5.	OGATAT	[Cu($H_2$4py-Ris)]	$P\bar{1}$	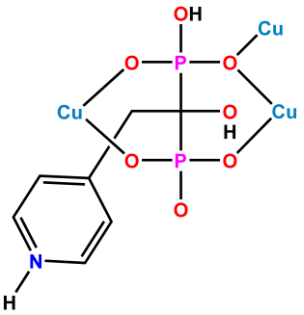	Y.-S. Ma *et al.*, *RSC Adv.*, **3** (2013) 18430-18440
6.	OXAMUW	[Mn(H_2Zol)]·H_2O	$P2_1/c$	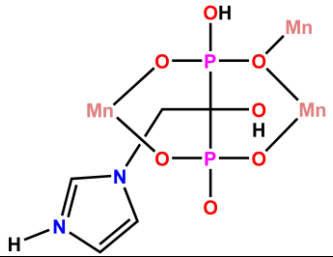	D.-K. Cao *et al.*, *Inorg. Chem.*, **50** (2011) 2278-2287
Coordination mode IIb					
1.	KEVVOX01	[Cu(H_2Pam)]·H_2O	$P2_1/c$	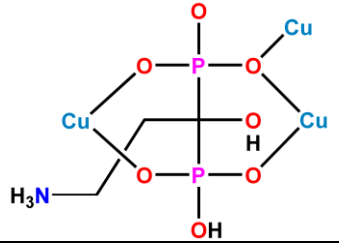	G. Li *et al.*, *J. Coord. Chem.*, **61** (2008) 540-549

Coordination mode III					
1.	DUPXOC	[Zn(H_2Ris)]	$P2_1/n$	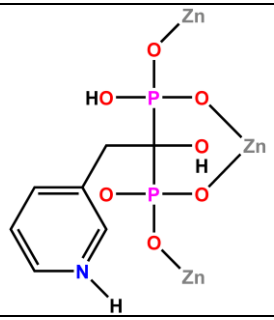	X. Huang *et al.*, *Acta Cryst.*, E**66** (2010) m59-m60
Coordination mode IV					
1.	HIRJUP	[Fe(H_2Ris)(H_2O)]	$P2_1/n$	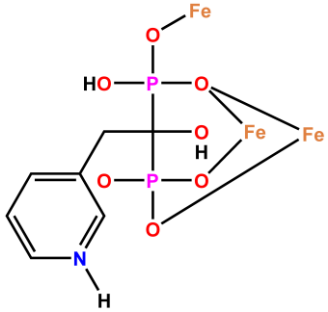	K.-R. Ma *et al.*, *Synth. Met.*, **182** (2013) 40-48
2.	MINKEA	[Co(H_2Ris)(H_2O)]	$P2_1/n$	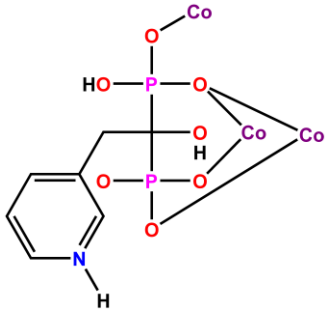	Z.-C. Zhang *et al.*, *Dalton Trans.*, **0** (2007) 4681-4684

3.	PUNZII	[Mn(H_2Ris)(H_2O)]	$P2_1/n$	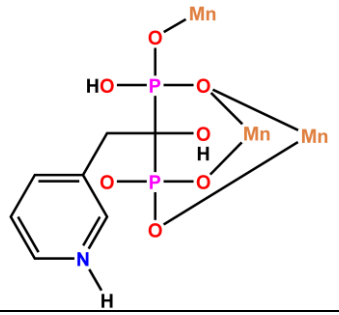	J. Zhao *et al.*, *Inorg. Chim. Acta*, **363** (2010) 662-668
Coordination mode V					
1.	TAMMAX	[Ca(H_2Pam)(H_2O)]·H_2O	$Pna2_1$	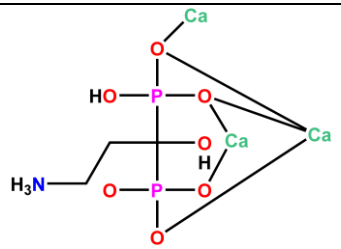	D. Liu *et al.*, *Chem. Commun.*,**48** (2012) 2668-2670
2.	TAMMEB	[Ca(H_2Zol)(H_2O)]	$Pna2_1$	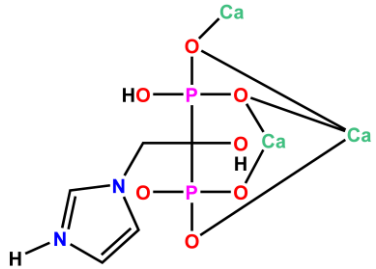	D. Liu *et al.*, *Chem. Commun.*, **48** (2012) 2668-2670

[a]Abbreviations: H_4Ale – alendronic acid, H_4Pam – pamidronic acid, H_4Ris – risedronic acid, $H_4$4Py-Ris – 1-hydroxy-2-(4-pyridyl)etylidene-1,1-diphosphonic acid, H_4Zol – zoledronic acid

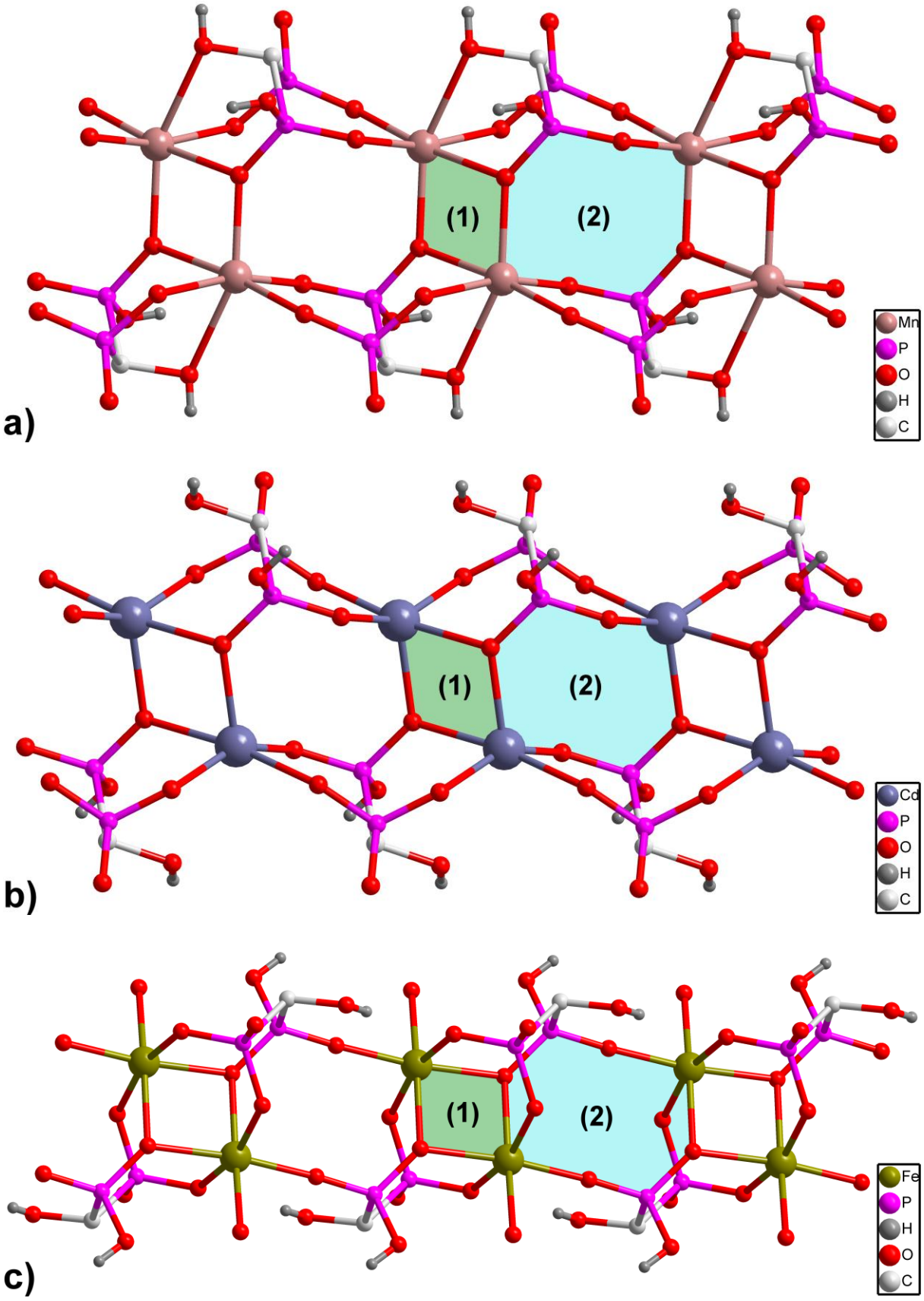
a)
(1)
(2)
Mn
P
O
H
C
b)
(1)
(2)
Cd
P
O
H
C
c)
(1)
(2)
Fe
P
H
O
C

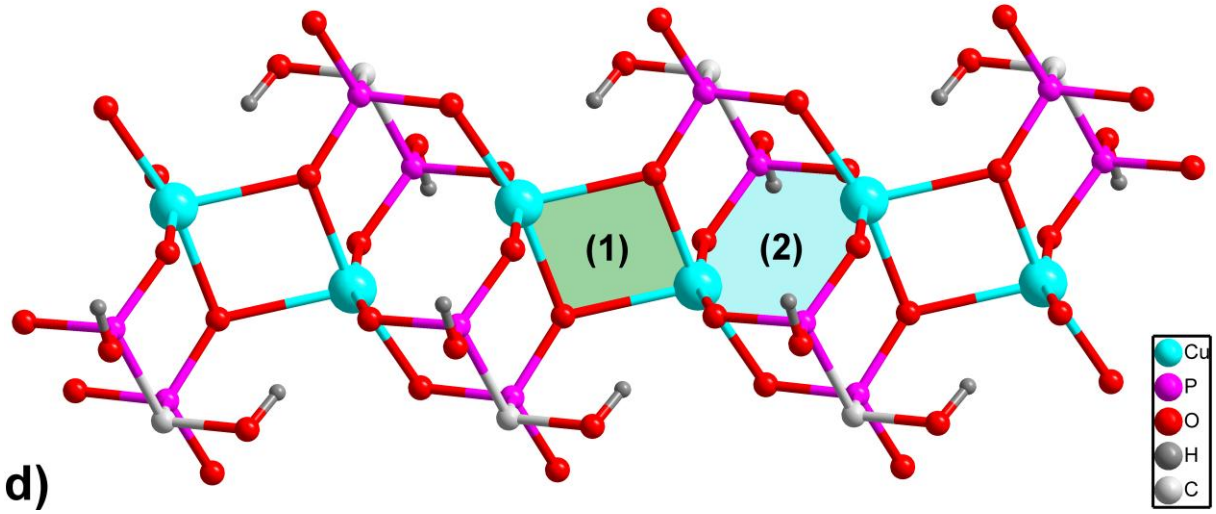

Figure S1. The family of BPs-based coordination polymers with 1:1 metal-to-ligand stoichiometry displaying 1D ladder-type coordination chains with common 4- and 8-membered ring systems connecting metal centres through μ_2-O and O–P–O bridges (marked as 1 and 2, respectively). (a) The architecture of 1D chain of representative $[Mn(H_2Ris)]\cdot 3H_2O$ complex (Refcode YUDPAP, observed also in: ODEPEV, GIKPEW, XEHTG and XEHTEK, Table S1) based on six-coordinated metal centre with coordinated hydroxyl oxygen atom. (b) The ladder architecture in representative $[Cd(H_2Ris)]\cdot H_2O$ complex (Refcode GAPSIC, observed also in: ODEPAR, OGASOG, OGATUN and OXAMUW, Table S1) based on five-coordinated metal centre with hydroxyl oxygen atom remaining uncoordinated. (c) The double μ_2-O and double O–P–O bridged dimeric core in representative $[Fe(H_2Ris)(H_2O)]$ complex (Refcode HIRJUP, observed also in: MINKEA and PUNZII, Table S1) resulting from the replacement of the hydroxyl oxygen atom with a water molecule in metal coordination sphere. (d) The formation of linear chain architecture displayed by representative $[Cu(H_2Pam)]\cdot H_2O$ complex (Refcode KEVVOX01, observed also in: OGATAT, Table S1) caused by the different arrangement of five-coordinated metal core compared to structures gathered in point b.

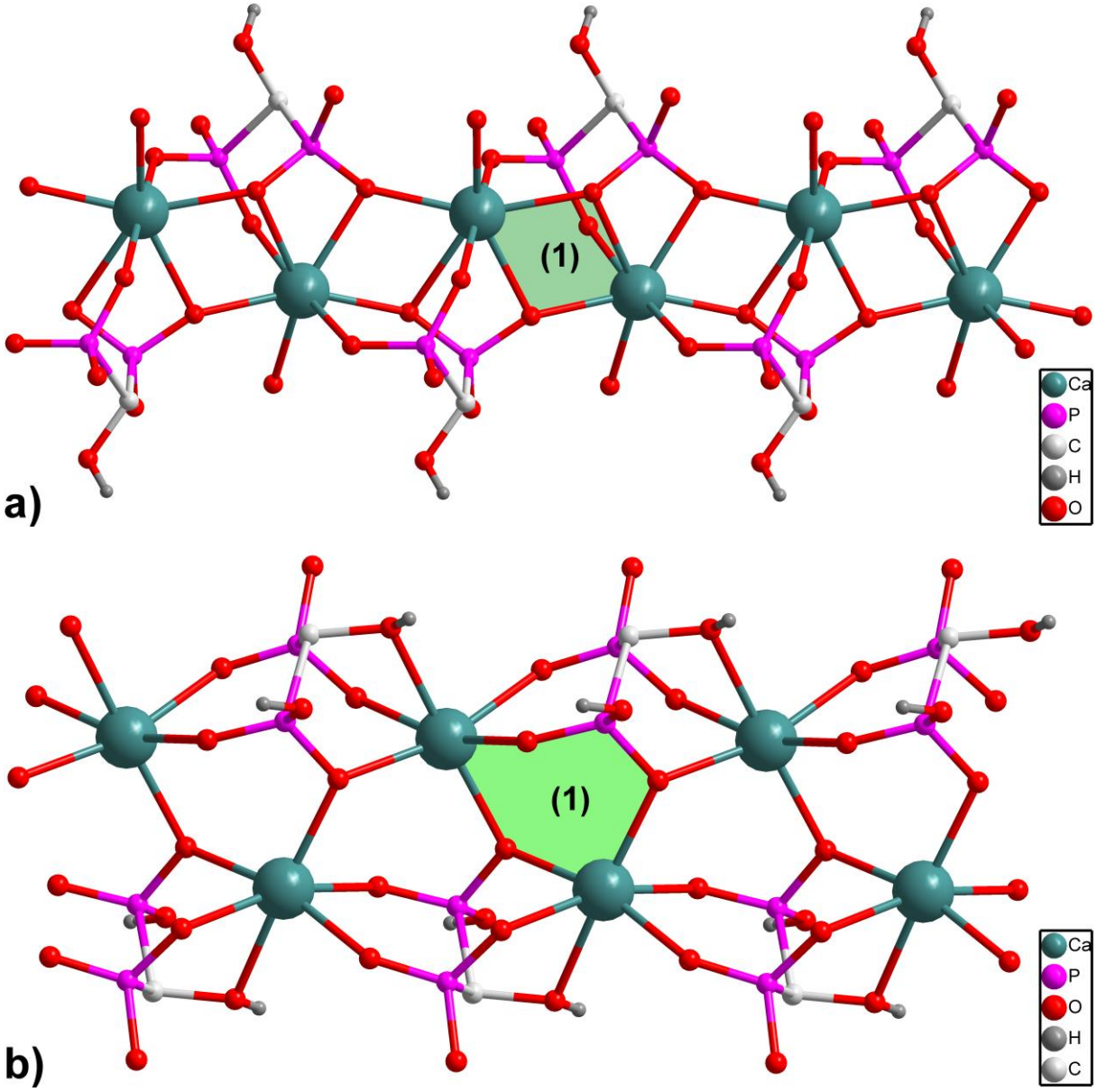

Figure S2. The schematic representation of *zig-zag* chain structures observed in BPs-based Ca(II) coordination polymers. (a) The seven-coordinate Ca(II) centres linked through μ_2-O phosphonate bridges into 4-membered ring (marked as 1) in representative $[Ca(H_2Pam)(H_2O)]\cdot H_2O$ complex (Refcode TAMMAX, observed also in: TAMMEB, Table S1). (b) The propagation of dimeric units into coordination chains in the $[Ca(H_2Ale)]\cdot H_2O$ complex (Refcode LILQII, Table S1). The lower coordination number of Ca(II) ion and replacement of the water molecule with the hydroxyl oxygen atom in metal coordination sphere resulting in formation of 6-membered rings (marked as 1) connecting metal centres by the mixed phosphonate O–P–O and μ_2-O bridges.

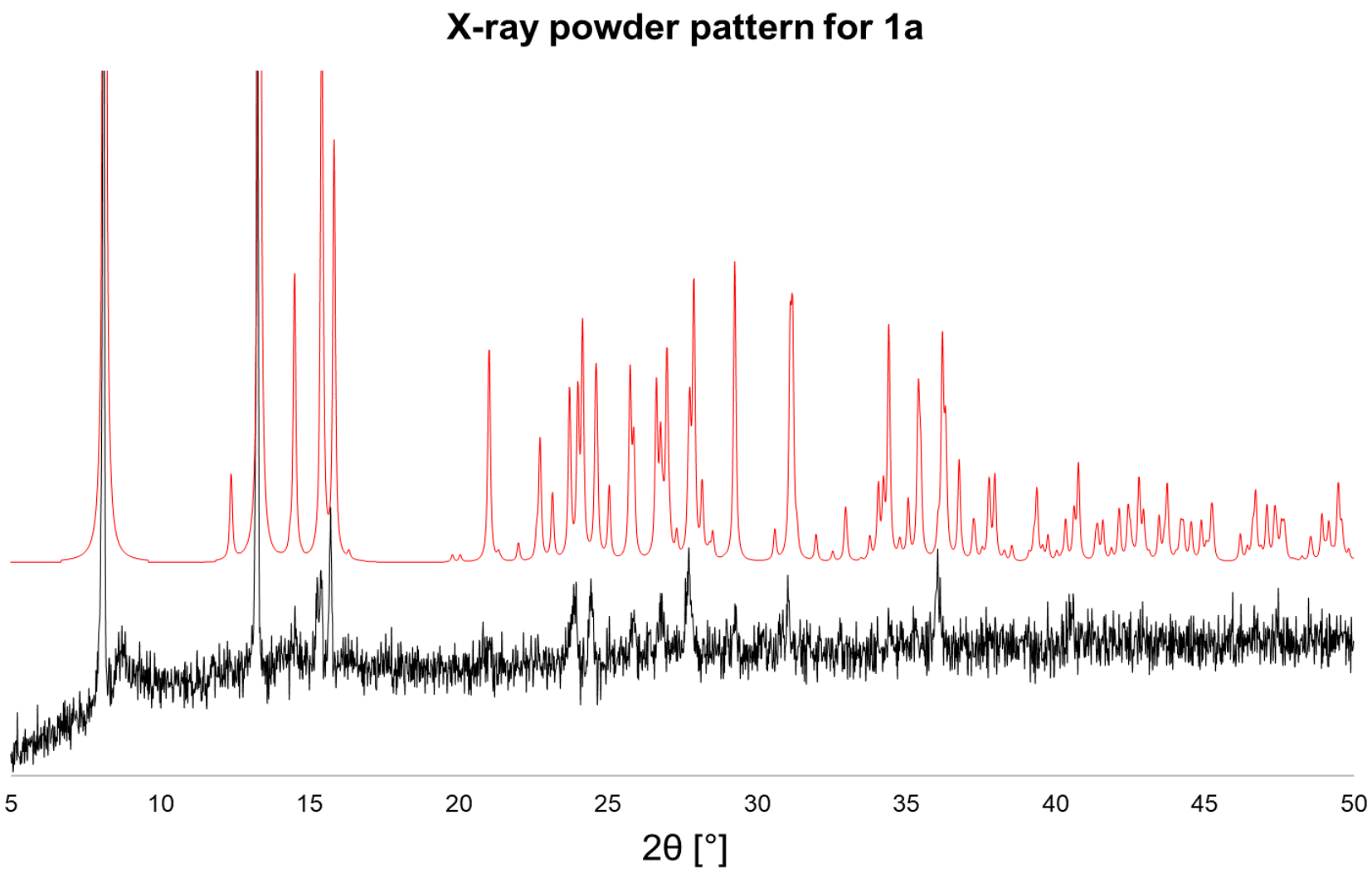

Figure S3. Experimental X-ray powder pattern (black, T = 298 K, Cu-Kα1) and simulated powder pattern (red, T = 80 K, Mo-Kα) based on the results from single-crystal X-ray diffraction for the complex **1a**.

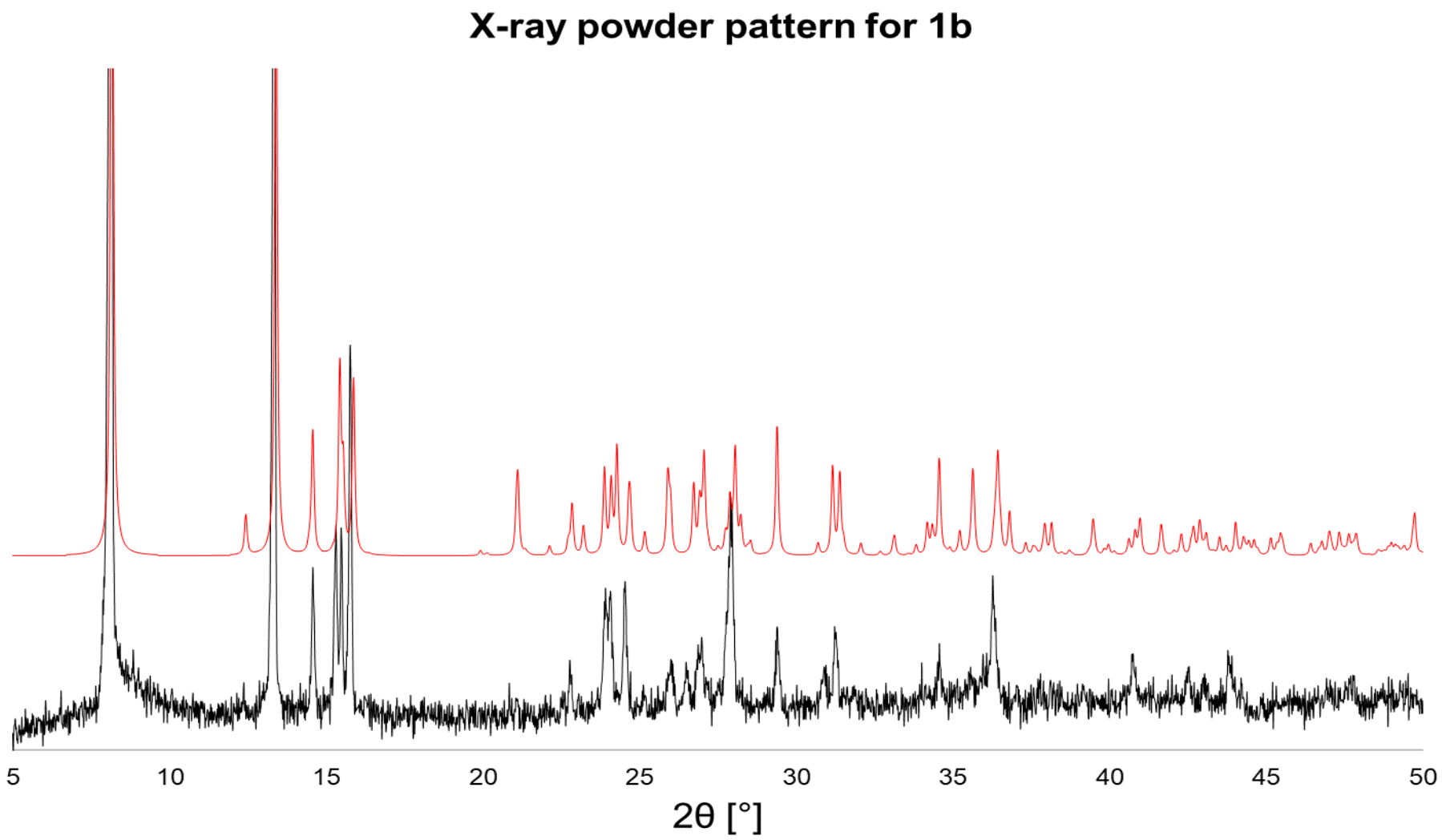

Figure S4. Experimental X-ray powder pattern (black, T = 298 K, Cu-Kα1) and simulated powder pattern (red, T = 80 K, Mo-Kα) based on the results from single-crystal X-ray diffraction for the complex **1b**.

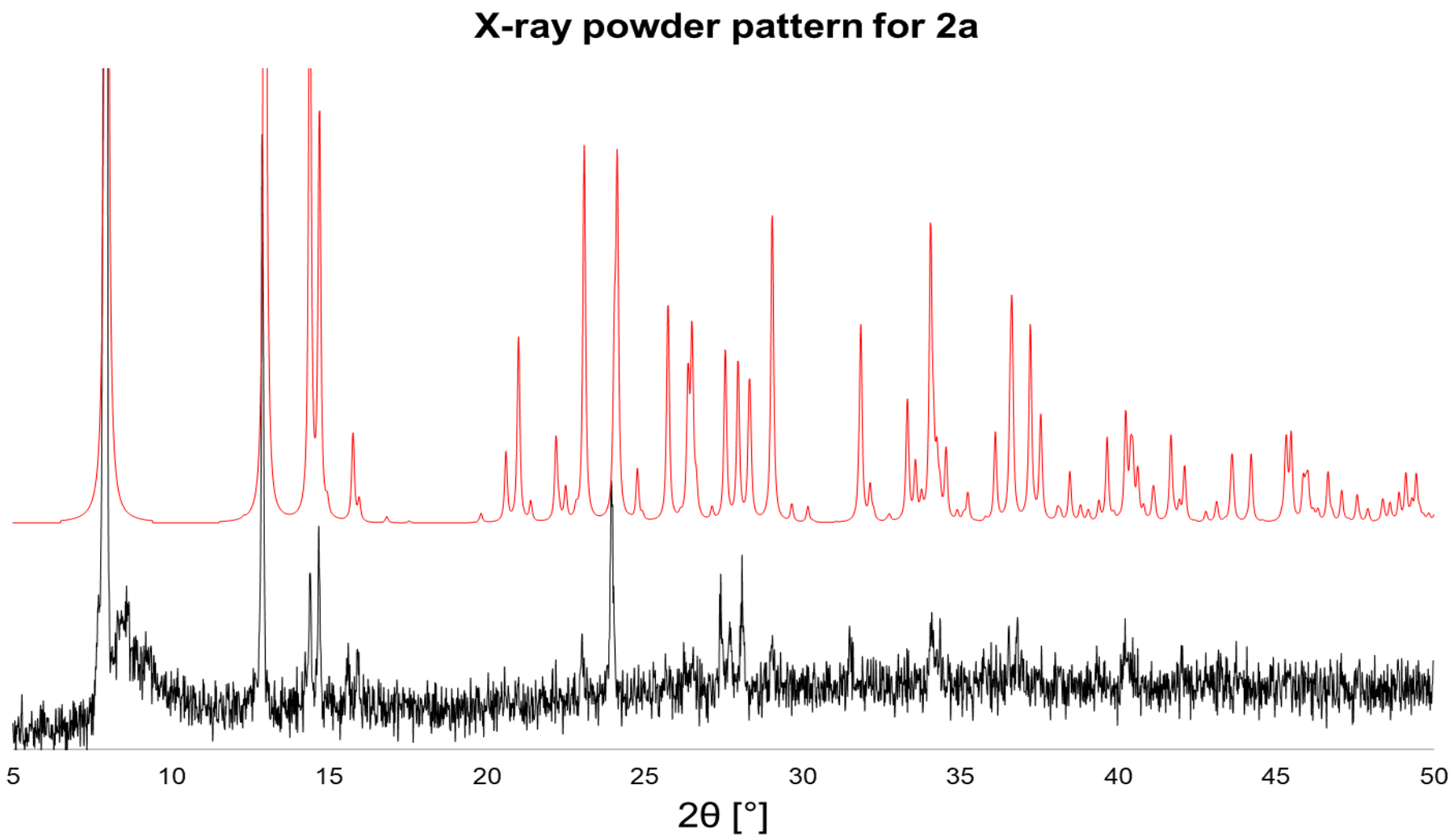

Figure S5. Experimental X-ray powder pattern (black, T = 298 K, Cu-Kα1) and simulated powder pattern (red, T = 80 K, Mo-Kα) based on the results from single-crystal X-ray diffraction for the complex **2a**.

Table S2. Selected interatomic distances (Å), bond angles (°) and torsion angles (°) for the compounds **1a**, **1b** and **2a**.

	1a	**1b**	**2a**
Bond lengths			
P1–O1	1.498(2)	1.502(4)	1.4955(15)
P1–O2	1.512(2)	1.515(4)	1.5153(16)
P1–O3	1.579(2)	1.577(4)	1.5798(16)
P2–O4	1.517(2)	1.507(4)	1.5204(15)
P2–O5	1.523(2)	1.528(4)	1.5226(16)
P2–O6	1.539(2)	1.544(4)	1.5401(16)
Bond angles			
N1–C2–C1	115.5(2)	115.2(4)	110.32(17)
O1–P1–O2	117.39(12)	117.9(2)	117.88(9)
O1–P1–O3	105.77(12)	105.6(2)	107.07(9)
O2–P1–O3	111.53(11)	111.5(2)	110.74(9)
O4–P2–O5	112.58(12)	112.9(2)	112.73(9)
O4–P2–O6	112.76(11)	113.6(2)	112.67(8)
O5–P2–O6	113.01(11)	112.6(2)	112.80(9)
Torsion angles			
O7–C1–C2–N1	165.1(2)	165.3(4)	-172.66(15)
P1–C1–C2–N1	-81.2(2)	-81.2(5)	-59.03(18)
P2–C1–C2–N1	44.6(3)	45.1(6)	68.34(19)
O7–C1–C2–C3	-49.5(3)	-50.0(6)	-43.1(2)
P1–C1–C2–C3	64.2(3)	63.4(6)	70.49(19)
P2–C1–C2–C3	-170.1(2)	-170.3(4)	-162.14(14)
O7–C1–C2–C4	20.8(3)	21.3(7)	-
P1–C1–C2–C4	134.5(2)	134.7(4)	-
P2–C1–C2–C4	-99.8(3)	-99.0(5)	-
O7–C1–C2–C5	-	-	58.3(2)
P1–C1–C2–C5	-	-	171.93(14)
P2–C1–C2–C5	-	-	-60.7(2)

Table S3. Selected interatomic distances (Å) and bond angles (°) for the compounds **1a**, **1b** and **2a**.

	1a [M = Co(II)]	**1b** [M = Ni(II)]		**2a** [M = Co(II)]
Bond lengths (Å)				
M1–O4^{i}	2.023(2)	2.028(4)	M1–O4^{iii}	2.0419(15)
M1–O2	2.081(2)	2.064(4)	M1–O2	2.0666(15)
M1–O1^{ii}	2.071(2)	2.048(4)	M1–O1^{iv}	2.0734(15)
M1–O1*W*	2.1161(19)	2.060(3)	M1–O1*W*	2.1640(17)
M1–O6	2.183(2)	2.145(4)	M1–O6	2.1773(15)
M1–O7	2.1888(18)	2.125(3)	M1–O7	2.1946(17)
Bond angles (°)				
O4^{i}–M1–O2	171.79(8)	173.47(16)	O4^{iii}–M1–O2	175.85(6)
O4^{i}–M1–O1^{ii}	92.69(8)	91.15(15)	O4^{iii}–M1–O1^{iv}	90.90(6)
O2–M1–O1^{ii}	89.88(8)	90.09(16)	O2–M1–O1^{iv}	91.51(6)
O4^{i}–M1–O1*W*	92.10(8)	92.46(15)	O4^{iii}–M1–O1*W*	95.47(6)
O2–M1–O1*W*	95.77(8)	93.97(15)	O2–M1–O1*W*	87.75(6)
O1^{ii}–M1–O1*W*	88.28(8)	89.23(15)	O1^{iv}–M1–O1*W*	93.59(6)
O4^{i}–M1–O6	91.34(8)	92.07(15)	O4^{iii}–M1–O6	90.97(6)
O2–M1–O6	86.17(8)	86.68(14)	O2–M1–O6	86.35(6)
O1^{ii}–M1–O6	175.96(8)	176.76(17)	O1^{iv}–M1–O6	174.96(6)
O1*W*–M1–O6	91.27(8)	90.95(14)	O1*W*–M1–O6	90.89(6)
O4^{i}–M1–O7	89.38(8)	89.43(15)	O4^{iii}–M1–O7	92.01(6)
O2–M1–O7	82.48(8)	84.05(14)	O2–M1–O7	84.36(6)
O1^{ii}–M1–O7	100.45(8)	97.95(14)	O1^{iv}–M1–O7	96.53(6)
O1*W*–M1–O7	171.08(7)	172.54(16)	O1*W*–M1–O7	167.32(6)

Symmetry codes: (i) –*x*+1, –*y*+1, –*z*+1; (ii) –*x*+2, –*y*+2, –*z*+1; (iii) −*x*+1/2, −*y*+3/2, −*z*+1; (iv) −*x*+1/2, −*y*+1/2, −*z*+1.

Table S4. (a) Proposed hydrogen bonds for **1a**, **1b** and **2a**.

D–H···*A*	*D*–H		H···*A*		*D*···*A*		*D*–H···*A*	
Compound	***1a***	***1b***	***1a***	***1b***	***1a***	***1b***	***1a***	***1b***
O3–H3···O5	0.84	0.84	1.80	1.79	2.602(3)	2.586(5)	159	157
O7–H7···O6^{i}	0.84	0.84	1.87	1.89	2.703(3)	2.714(5)	169	166
C3–H3*A*···O5^{v}	0.99	0.99	2.60	2.56	3.350(4)	3.325(6)	133	134
C4–H4*B*···O3^{vi}	0.99	0.99	2.60	2.58	3.566(4)	3.540(7)	164	164
N2–H2···O5^{vii}	0.88	0.88	1.82	1.82	2.682(3)	2.683(6)	166	166
C21–H21···O2*W*^{i}	0.95	0.95	2.46	2.44	3.195(4)	3.185(7)	135	135
C41–H41···O1^{viii}	0.95	0.95	2.60	2.56	3.493(4)	3.468(6)	158	159
C51–H51···O2*W*^{ii}	0.95	0.95	2.52	2.51	3.374(4)	3.359(7)	149	148
O1*W*–H1*W*···O6^{ix}	0.84	0.84	2.23	2.25	2.950(3)	2.945(5)	143	140
O1*W*–H2*W*···O2^{ix}	0.84	0.84	2.05	2.03	2.806(3)	2.784(5)	150	149
O2*W*–H3*W*···O5^{ix}	0.84	0.84	2.39	2.47	3.227(3)	3.229(6)	174	150
O2*W*–H4*W*···O1^{ii}	0.84	0.84	2.30	2.27	3.075(3)	3.093(6)	154	165
Compound ***2a***								
O3–H3···O5	0.84		1.80		2.611(2)		163	
O7–H7···O6^{iii}	0.84		1.89		2.698(2)		161	
N2–H2*N*···O5^{x}	0.88		1.79		2.666(2)		174	
C3–H3*A*···O5^{xi}	0.99		2.53		3.289(3)		134	
C5–H5*A*···O1*W*^{iii}	0.99		2.41		3.239(3)		141	
C21–H21···O2*W*^{iv}	0.95		2.25		3.154(3)		158	
C41–H41···O3^{xiii}	0.95		2.47		3.206(3)		134	
O1*W*–H1*W*···O6^{xii}	0.84		2.46		3.102(2)		134	
O1*W*–H2*W*···O2^{xii}	0.84		2.09		2.865(2)		153	
O2*W*–H3*W*···O1*W*	0.84		2.26		2.984(3)		145	
O2*W*–H4*W*···O4^{iii}	0.84		2.56		3.173(3)		130	

Symmetry codes: (i) −*x*+1, −*y*+1, −*z*+1; (ii) −*x*+2, −*y*+2, −*z*+1; (iii) −*x*+1/2, −*y*+3/2, −*z*+1; (iv) −*x*+1/2, −*y*+1/2, −*z*+1; (v) *x*, *y*+1, *z*; (vi) *x*−1, *y*, *z*; (vii) −*x*+1, −*y*+1, −*z*+2; (viii) −*x*+2, −*y*+2, −*z*+2; (ix) −*x*+2, −*y*+1, −*z*+1; (x) −*x*+1/2, *y*−1/2, −*z*+3/2; (xi) *x*+1/2, *y*−1/2, *z*; (xii) −*x*, −*y*+1, −*z*+1; (xiii) −*x*+1/2, *y*+1/2, −*z*+3/2

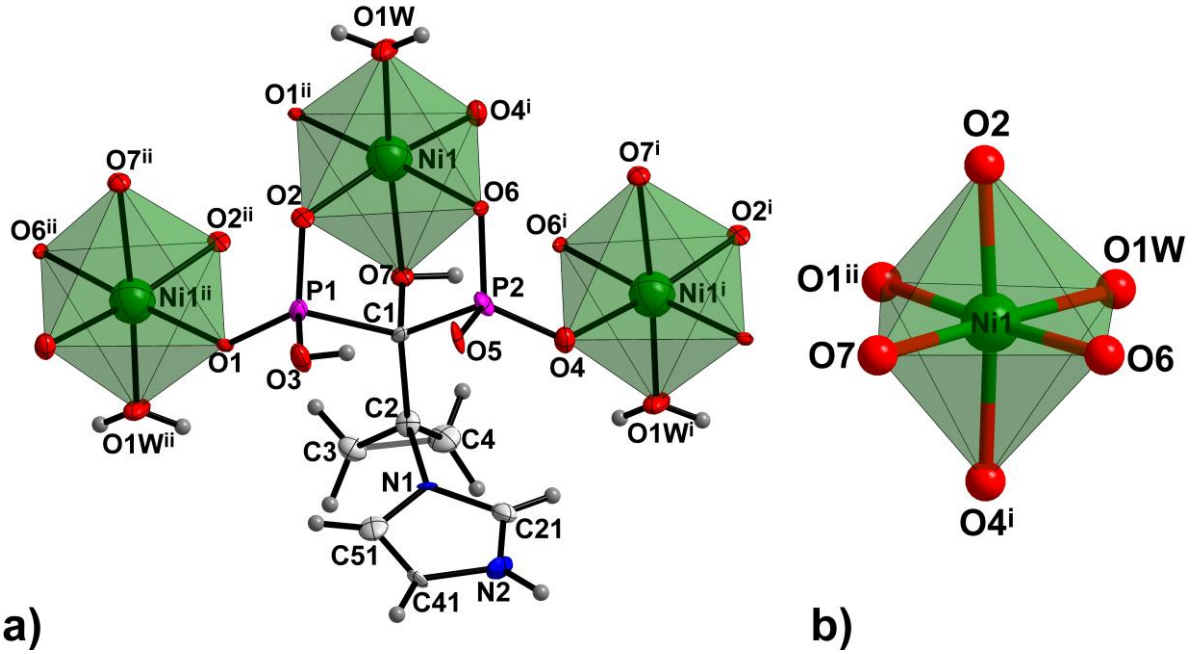

Figure S6. (a) The building unit and the atom-numbering scheme of complex **1b**. Lattice water molecule is omitted for clarity. Displacement ellipsoids except Ni1 atoms are drawn at 80% probability level. (b) Coordination environments of Ni1 center in **1b**. Symmetry codes are given in Table S3.

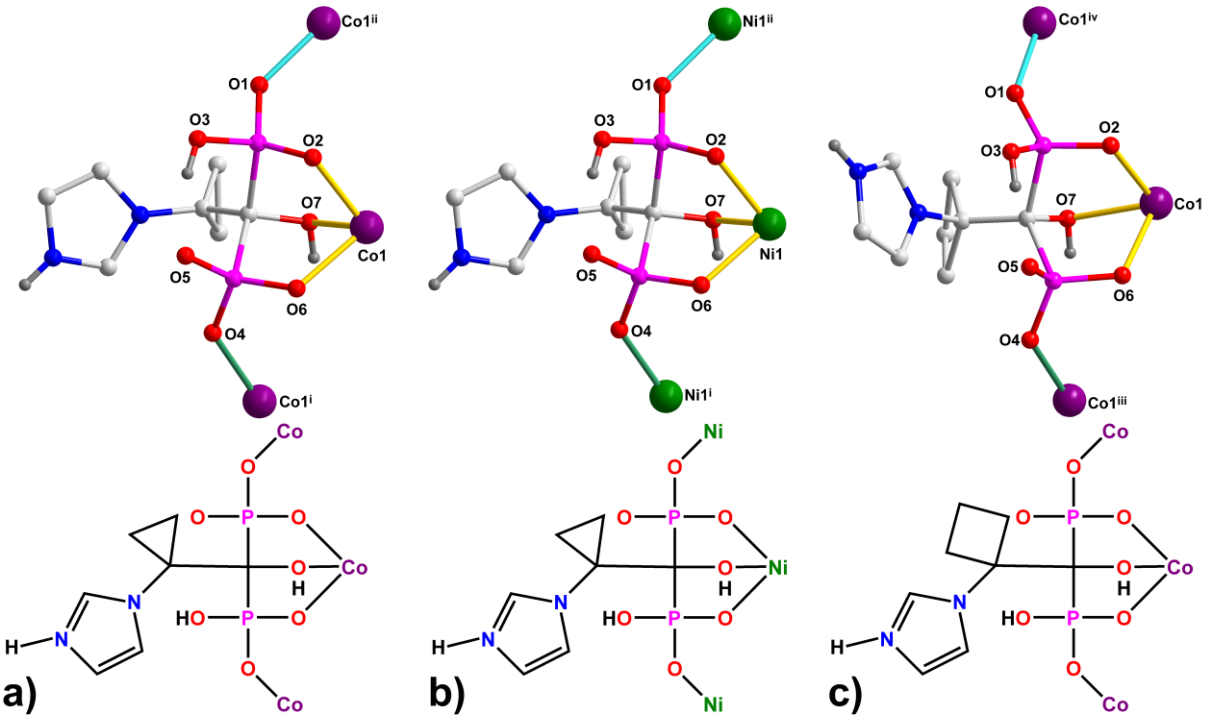

Figure S7. Coordination modes of H_2cppZol^{2-} and H_2cbtZol^{2-} (above) and its schematic representation (below) in (a) **1a**, (b) **1b** and (c) **2a**. All C-bound H-atoms are omitted for clarity. Symmetry codes are given in Table S3.

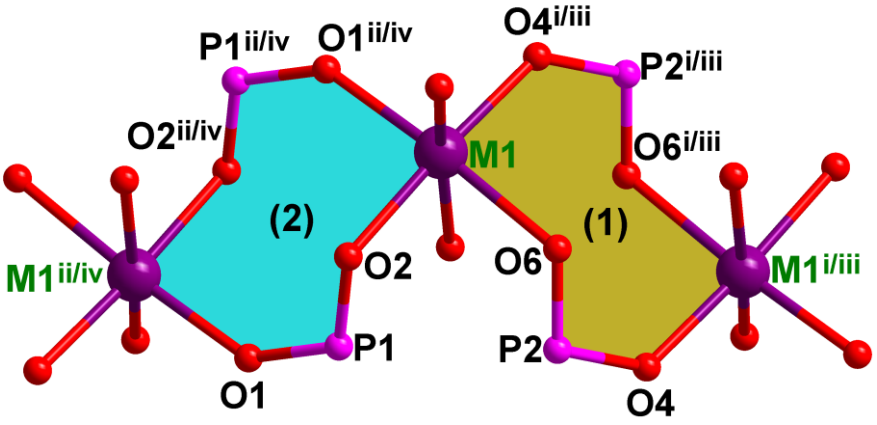

Figure S8. Connection of M(II) centres (M = Co in **1a** and **2a**, M = Ni in **1b**) leading to the formation of two 8-membered rings (1 and 2) with M1···M1$^{i/iii}$ and M1···M1$^{ii/iv}$ distances of 4.850(3) and 4.841(3) Å in **1a**, 4.797(3) and 4.841(3) Å in **1b** and 4.822(2) and 4.859(2) Å in **2a** across the O–P–O bridge, respectively. Symmetry codes are given in Table S3.

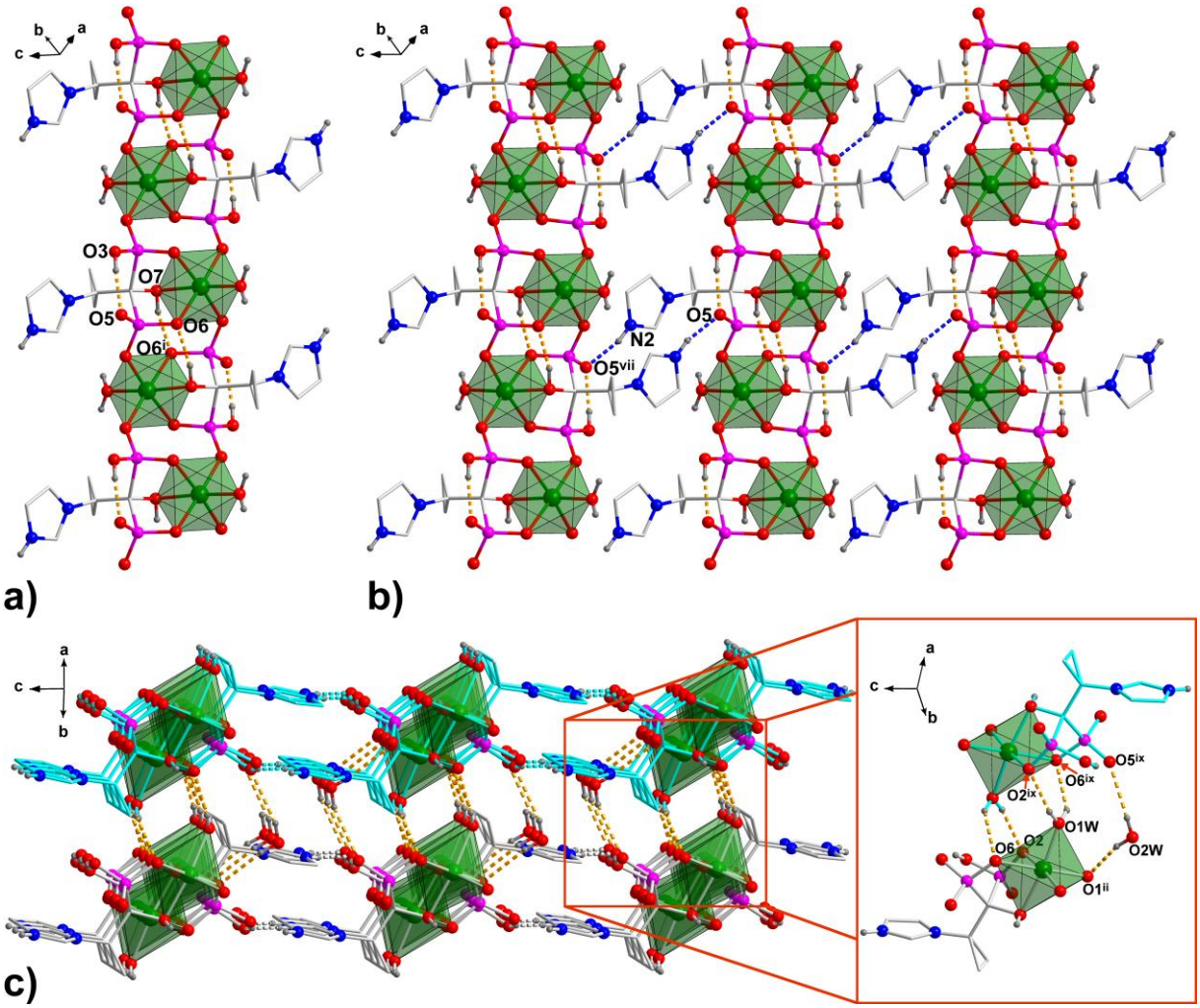

Figure S9. The packing diagram of the coordination polymer **1b**. (a) 1D polymeric chain running along [110] crystallographic direction; (b) Chains organized into 2D layer by N–H···O hydrogen bonds (blue dashed lines); (c) 3D supramolecular network formed through connection of adjacent layers by O–H···O hydrogen bonds (orange, dashed line) between coordinated or lattice water molecules and phosphonate O-atoms (details shown in the red frame). All C-bound H atoms not involved in the creation of hydrogen bonds and lattice water molecules (pictures a and b), are omitted for clarity. Symmetry codes are given in Table S4.

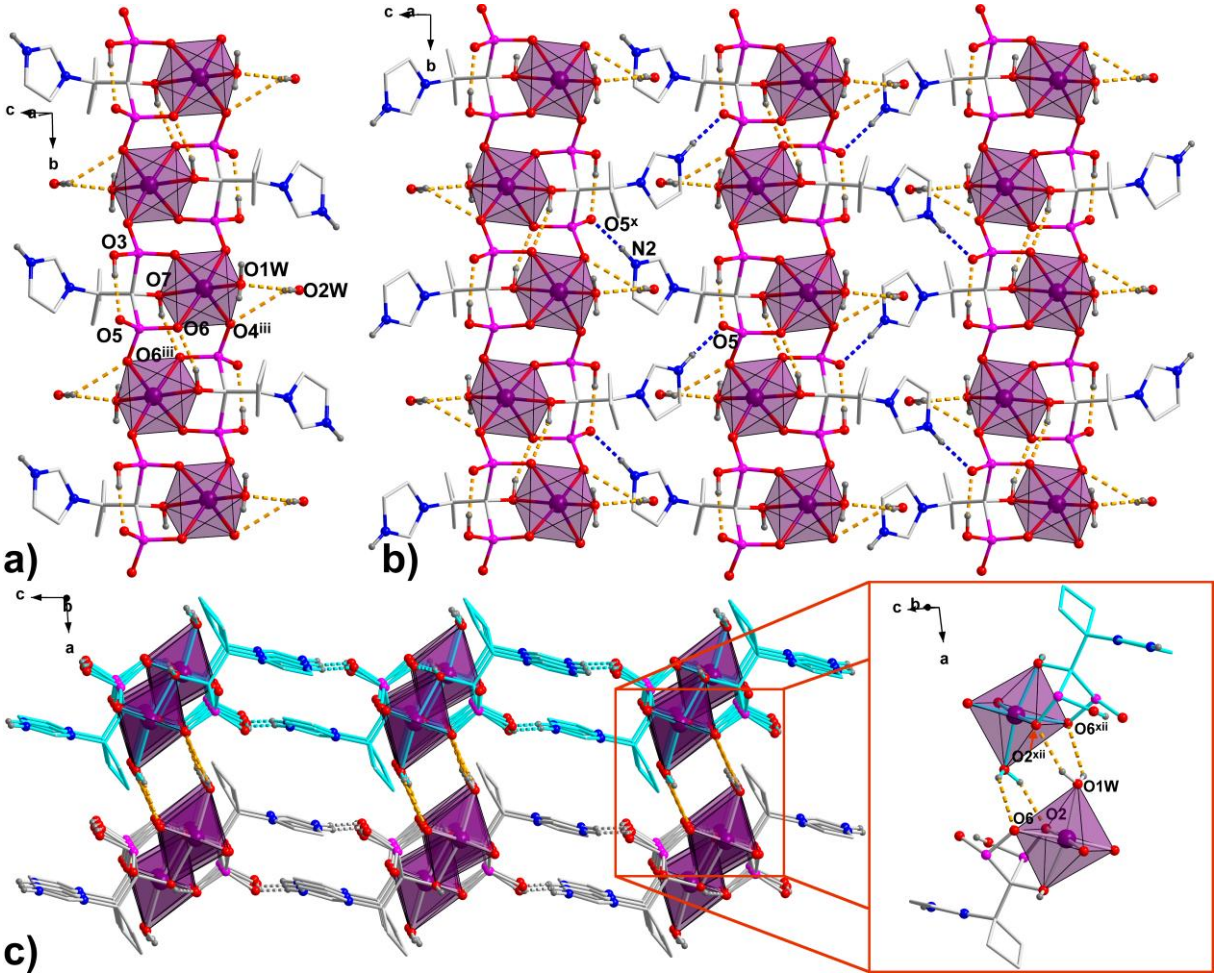

Figure S10. The packing diagram of the coordination polymer **2a**. (a) 1D polymeric chain running along *b* axis; (b) Chains organized into 2D layer by N–H···O hydrogen bonds (blue dashed lines); (c) 3D supramolecular network formed through connection of adjacent layers by O–H···O hydrogen bonds (orange, dashed line) between coordinated water molecules and phosphonate O-atoms (details shown in the red frame). All C-bound H atoms not involved in the creation of hydrogen bonds and lattice water molecules (picture c) are omitted for clarity. Symmetry codes are given in Table S4.

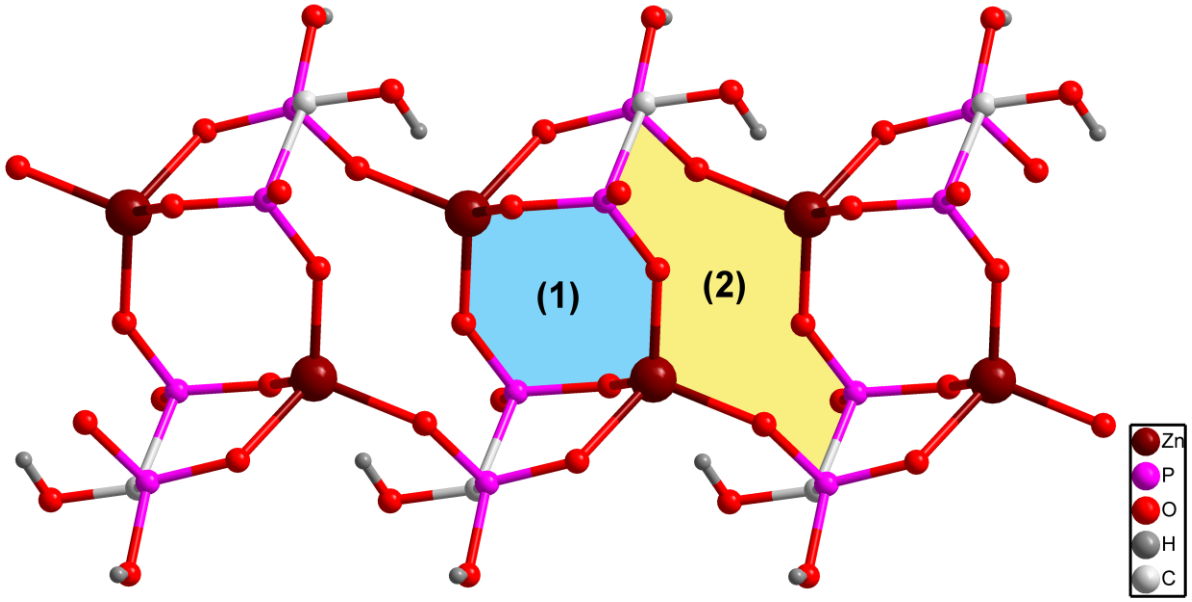

Figure S11. The schematic representation of the ladder chain architecture of 1D coordination polymer observed in [Zn(H_2Ris)] complex (Ref. DUPXOC, Table S1). The ladder is formed by connection of the four-coordinated Zn(II) centers through O–P–O and O–P–C–P–O bridges into alternating 8- and 12-membered rings (marked as 1 and 2).

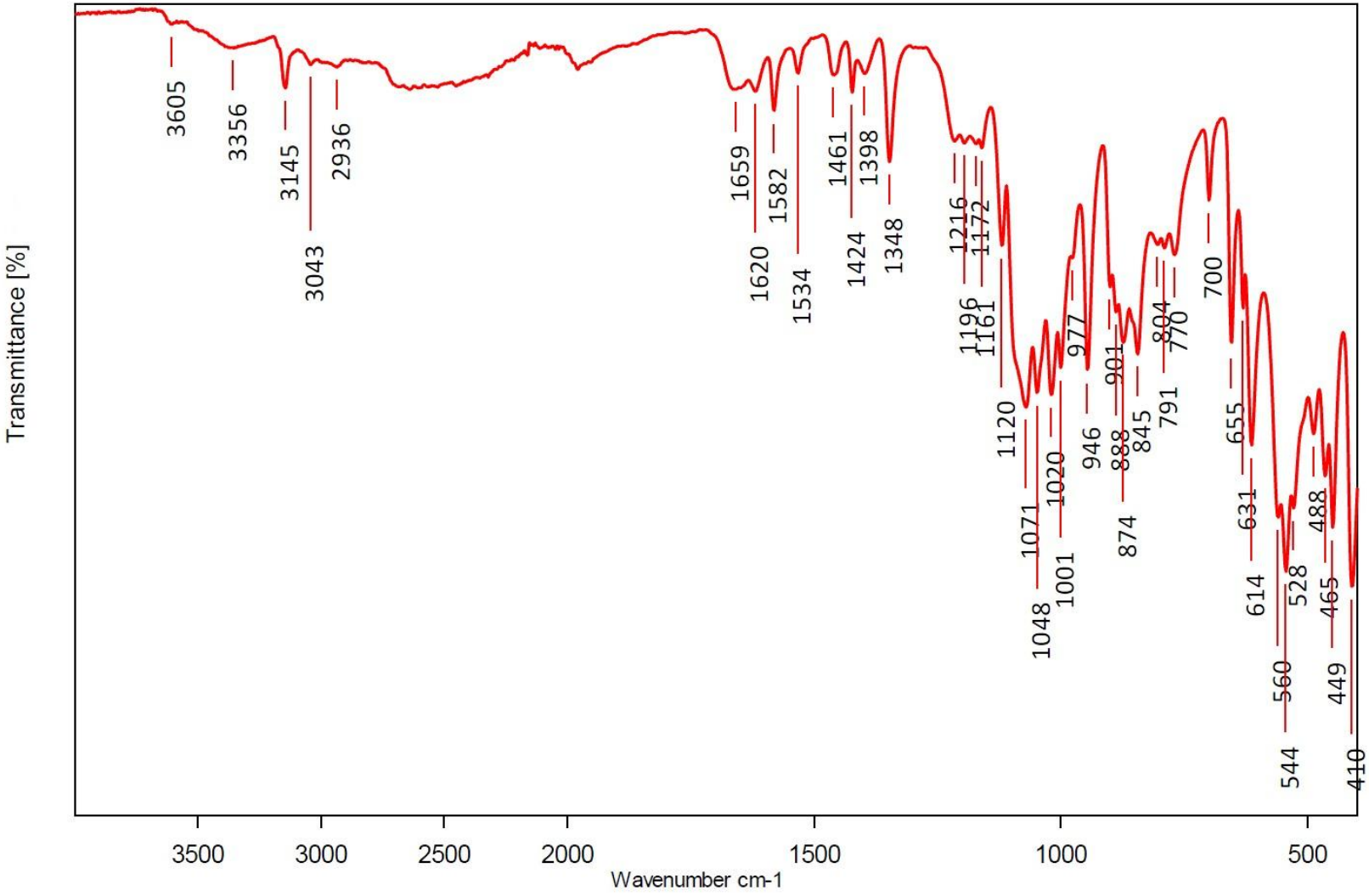

Figure S12. IR spectrum of **1a**.

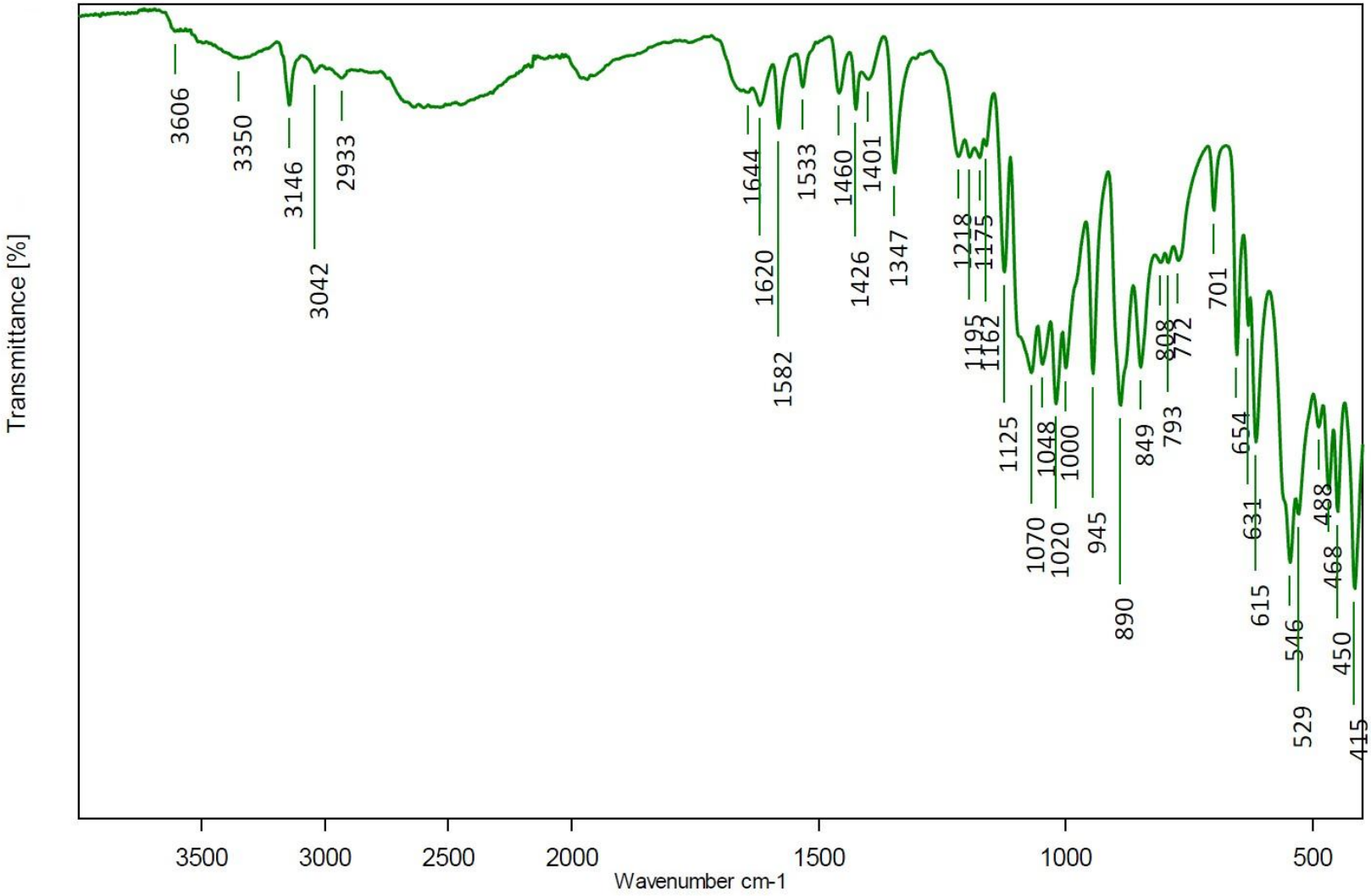

Figure S13. IR spectrum of **1b**.

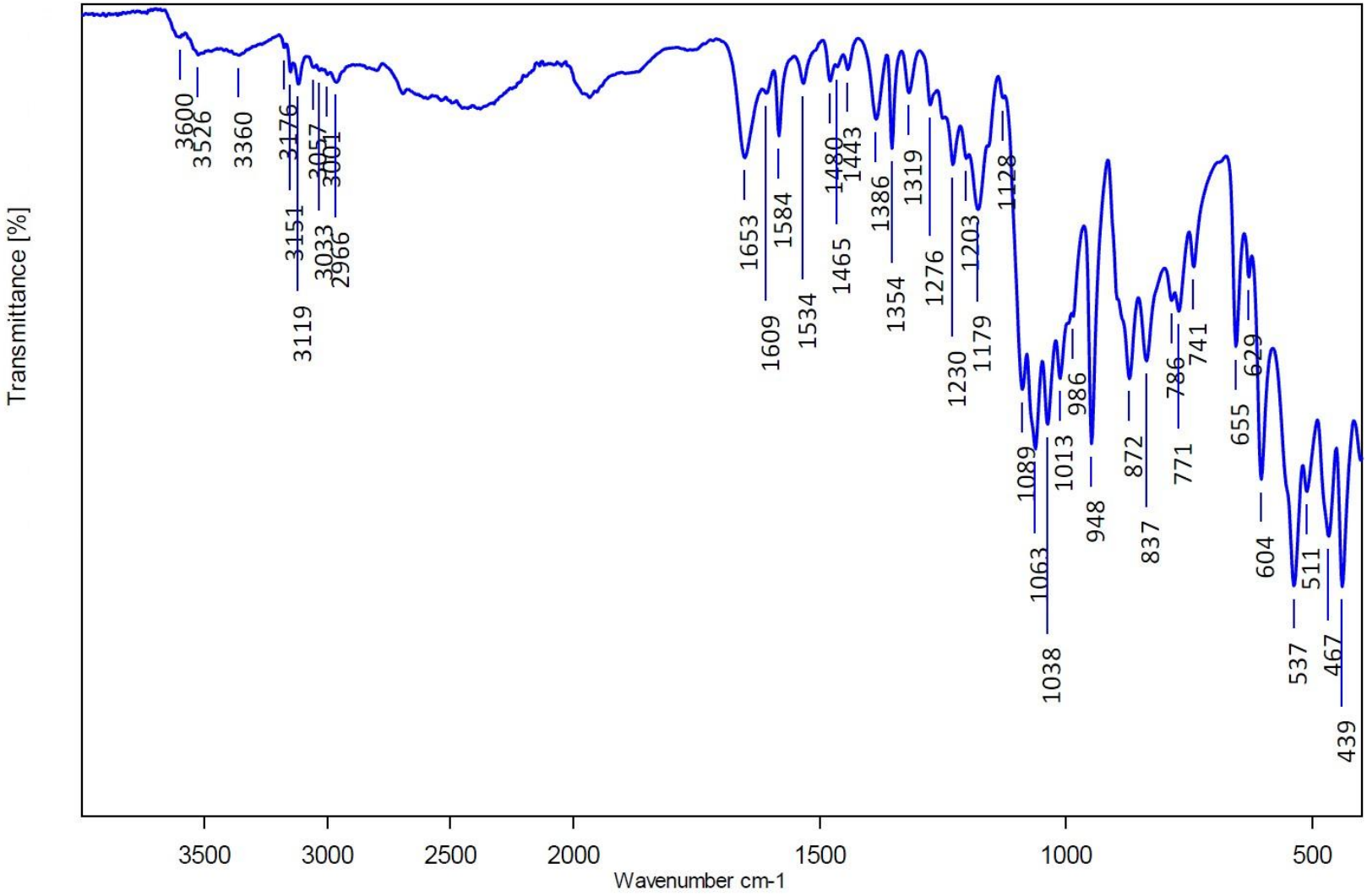

Figure S14. IR spectrum of **2a**.

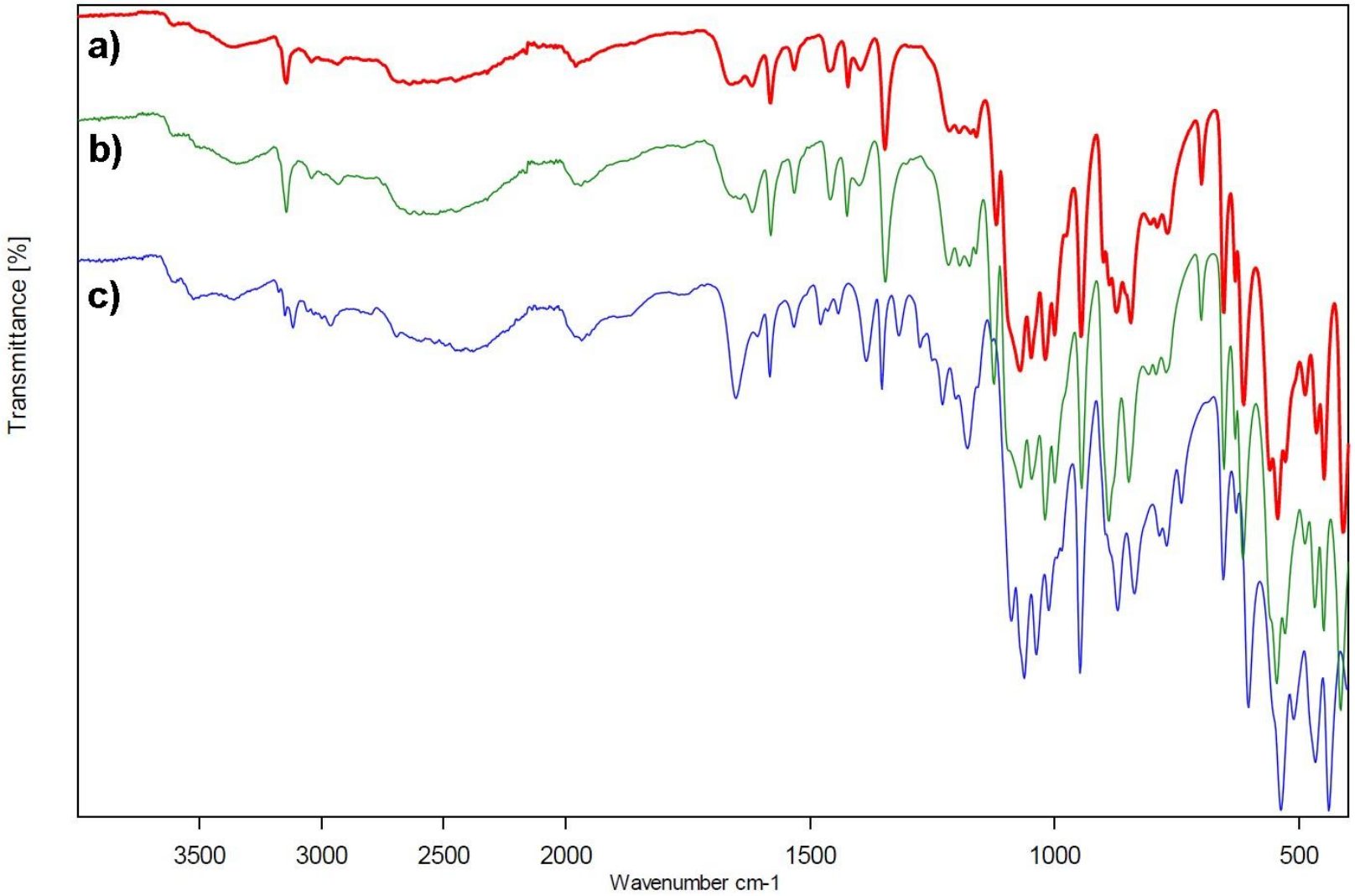

Figure S15. A comparison of IR spectra of (a) **1a**, (b) **1b** and (c) **2a**.

Table S5. Tentative assignments of the observed IR bands [cm^{-1}] for **1a**, **1b** and **2a**.

Wavenumber [cm^{-1}]			*Band assignment*[b]
1a	**1b**	**2a**	
3600-3200 br[a]	3600-3200 br	3600-3200 br	ν(O–H) (mostly O–H···O) ν(PO–H) ν(N–H)/im
3145	3146	3151 3119	ν(C–H)/im
3043 2936	3042 2933	3057 3033 3001 2966	$\nu_{s/as}$(C–H)/CH_2 (cyclopropyl/cyclobutyl ring)
1659 1620	1644 1620	1653 1609	δ(H_2O)
1582 1534	1582 1533	1584 1534	ν(C=C)/im, ν(N=C)/im, ν(N–C)/im, δ(C–H)/im
-	-	1480	δ(C–H)/CH_2 (cyclobutyl ring)
1461	1460	1465	δ(N–H)/im, ν(N–C)/im, ν(C–C)/im
1424	1426	1443	δ(C–H)/CH_2 (cyclopropyl/cyclobutyl ring)
1398	1401	1386	δ(CO–H)
1348	1347	1354 1319	δ(PO–H)
1216 1196 1172 1161	1218 1195 1175 1162	1276 1230 1203 1179	δ(C–H)/im, δ(N–H)/im δ(C–H)/CH_2 (cyclopropyl/cyclobutyl ring)
1120 1071	1125 1070	1128 1089	ν(P=O) ν(C–OH)
1048	1048	1063	δ(PO–H)
1020	1020	1038	ν(P=O)
1001	1000	1013	δ(CO–H) δ(C–H)/CH_2 (cyclopropyl/cyclobutyl ring)
946 901 888 874	945 890	948 872	ν(P–O) δ(PO–H)
845	849	837	ν(P–OH)
804 791 770	808 793 772	786 771 741	ν(C–P) ν(P–O)
700	701	-	$\rho_r(CH_2)$/cyclopropyl ring
655 631 614	654 631 615	655 629 604	π(im) δ(C–C) – cyclopropyl/cyclobutyl ring
560 544 528 488 465 449 410	546 529 488 450 415	537 511 467 439	δ(O–P–O) δ(C–P)

[a]br – broad; [b]ν_a – antisymmetric stretching; ν_s – symmetric stretching; δ – bending in-plane;π – bending out of plane, ρ_r – rocking.

Theoretical (DFT) calculations of H_4cppZol ligand

The DFT calculations were performed with the use of B3LYP [1, 2] functional corrected with dispersion correction D3 [3] (B3LYP-D3) and combined basis sets LanL2DZ [4] for P atoms in conjunction with the D95V(d,p) [5] basis set for all other atoms. The optimized structures of H_4cppZol was calculated using in the optimization procedures initial geometries obtained by single crystal X-ray diffraction. Lattice water molecule has not been included in the calculations. All calculated structures correspond to energy minima on the potential energy surface, *i.e.* no imaginary frequencies. The potential energy distribution (PED) terms were calculated by the FCART06 program [6]. Normal vibrations and corresponding IR bands were characterized on the basis of PED results and additionally verified by atom displacement animation done by Chemcraft application [7]. DFT calculated results were converted into theoretical spectra using Chemcraft application with Lorentzian band shape and 10 cm^{-1} half band width. For easier comparison of the observed and calculated band positions, scaling factors were calculated for two separate regions according to the method based on a least-squares approach [8]. All computations were carried out with Gaussian09 set of programs [9].

[1] A. D. Becke, *J. Chem. Phys.*, 1993, **98**, 5648.

[2] C. Lee, W. Yang and R. G. Parr, *Phys. Rev. B*, 1988, **37**, 785.

[3] S. Grimme, J. Antony, S. Ehrlich and H. Krieg, *J. Chem. Phys.*, 2010, **132**, 154104.

[4] P. J. Hay and W. R. Wadt, *J. Chem. Phys.*, 1985, **82**, 299.

[5] T. H. Dunning Jr. and P. J. Hay, in *Modern Theoretical Chemistry*, Ed. H. F. Schaefer III, Vol. 3, Plenum, New York, 1976, 1.

[6] W. B. Collier, I. Magdo and T. D. Klots, *J. Chem. Phys.*, 1999, **110**, 5710.

[7] Chemcraft – graphical software for visualization of quantum chemistry computations. https://www.chemcraftprog.com

[8] N. J. Harris, *J. Phys. Chem.*, 1995, **99**, 14689.

[9] M. J. Frisch, G. W. Trucks, H. B. Schlegel, G. E. Scuseria, M. A. Robb, J. R. Cheeseman, G. Scalmani, V. Barone, B. Mennucci, G. A. Petersson, H. Nakatsuji, M. Caricato, X. Li, H. P. Hratchian, A. F. Izmaylov, J. Bloino, G. Zheng, J. L. Sonnenberg, M. Hada, M. Ehara, K. Toyota, R. Fukuda, J. Hasegawa, M. Ishida, T. Nakajima, Y. Honda, O. Kitao, H. Nakai, T. Vreven, J. A. Montgomery, Jr., J. E. Peralta, F. Ogliaro, M. Bearpark, J. J. Heyd, E. Brothers, K. N. Kudin, V. N. Staroverov, R. Kobayashi, J. Normand, K. Raghavachari, A. Rendell, J. C. Burant, S. S. Iyengar, J. Tomasi, M. Cossi, N. Rega, J. M. Millam, M. Klene, J. E. Knox, J. B.

Cross, V. Bakken, C. Adamo, J. Jaramillo, R. Gomperts, R. E. Stratmann, O. Yazyev, A. J. Austin, R. Cammi, C. Pomelli, J. W. Ochterski, R. L. Martin, K. Morokuma, V. G. Zakrzewski, G. A. Voth, P. Salvador, J. J. Dannenberg, S. Dapprich, A. D. Daniels, O. Farkas, J. B. Foresman, J. V. Ortiz, J. Cioslowski and D. J. Fox, Gaussian, Inc., Wallingford CT, 2009.

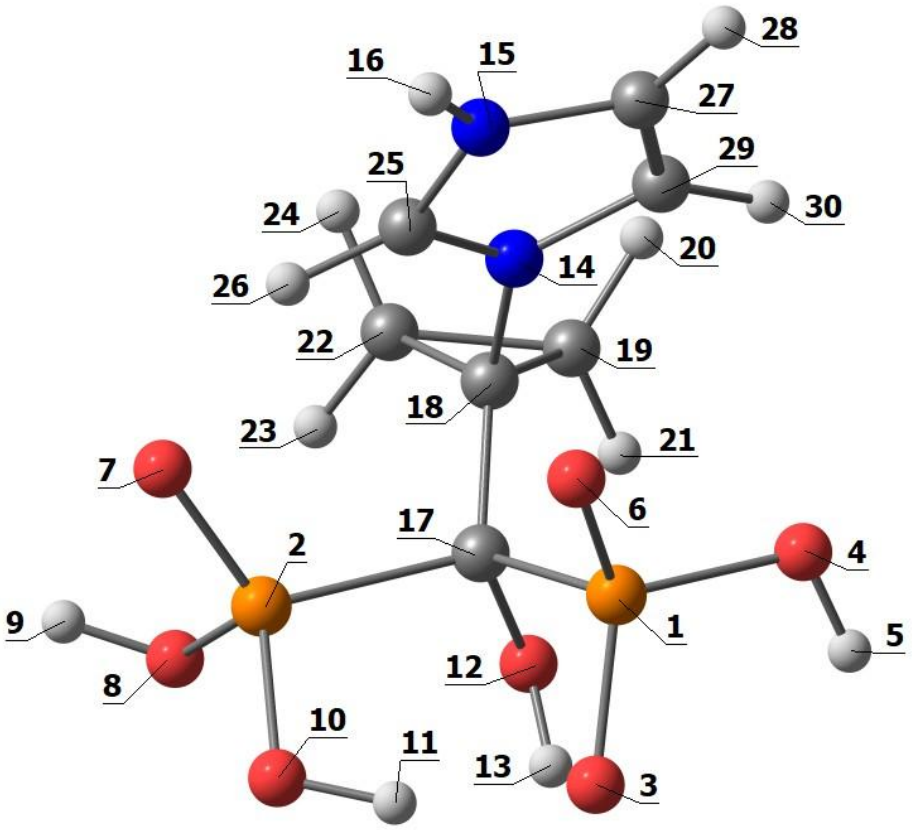

Figure S16. Optimized molecular geometry and the atom-numbering scheme of H_4cppZol ligand.

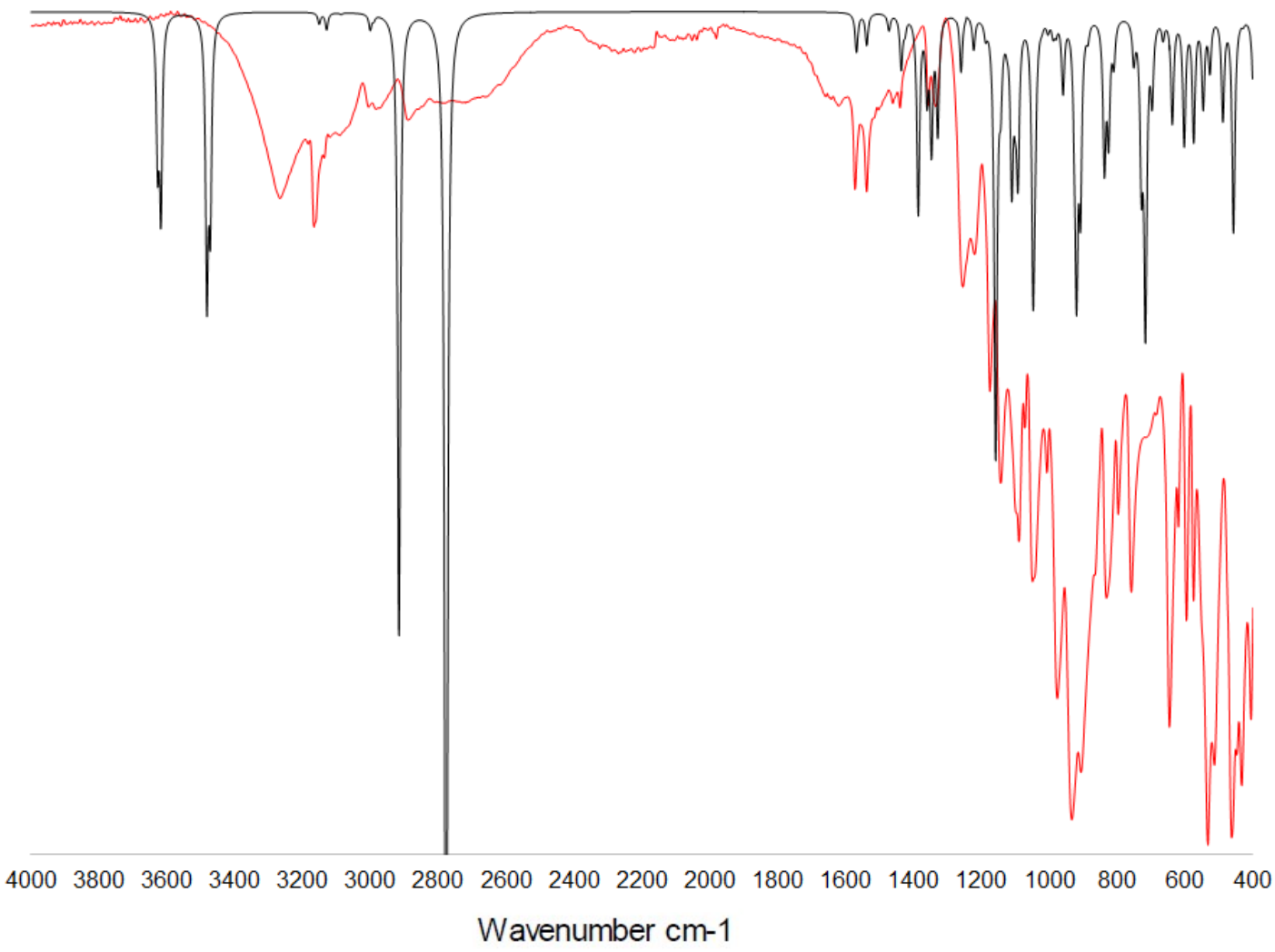

Figure S17. Comparison of experimental and the corresponding theoretical FT-IR spectrum (red and black line, respectively) of H_4cppZol ligand.

Table S6. Frequencies of theoretical and experimental IR bands and their vibrational assignments for H_4cppZol ligand.

No.	Calcd[a] ν [cm^{-1}]	Exp. ν [cm^{-1}]	General assignment[b,c]	Functional group	PED[d]
1.	3625	3265 br	ν(O–H)	phosphonate PO–H	ν(O4–H5)(99)
2.	3615		ν(O–H)	phosphonate PO–H	ν(O8–H9)(99)
3.	3479		ν(N–H)	imidazole	ν(N15–H16)(99)
4.	3470		ν(O–H)	hydroxyl CO–H	ν(O12–H13)(71)
6.	3149	3165	ν(C–H)	imidazole	ν(C29–H30)(70), ν(C27–H28)(28)
7.	3127	3135	ν(C–H)	imidazole	ν(C27–H28)(71), ν(C29–H30)(28)
8.	3100	3119	ν_{as}(C–H)	–CH_2–	ν(C19–H21)(60), ν(C19–H20)(27), ν(C22–H23)(6), ν(C22–H24)(5)
9.	3084	3089			ν(C22–H23)(51), ν(C22–H24)(36), ν(C19–H21)(9), ν(C19–H20)(4)
10.	2999	3004	ν_s(C–H)		ν(C19–H20)(67), ν(C19–H21)(29)
11.	2988	2982			ν(C22–H24)(57), ν(C22–H23)(40)
12.	2914	2889	ν(C–H)	imidazole	ν(C25–H26)(96)
13.	2775	n.o.	ν(O–H)	phosphonate PO–H	ν(O10–H11)(90)
14.	1567	1571	ν(C=C), ν(C–N), ν(C=N)	imidazole	ν(C27–C29)(81), ν(C25–N15)(7), ν(C25–N14)(6)
15.	1537	1537	ν(C–N), ν(C=N), δ(im)		ν(C25–N15)(41), ν(C25–N14)(22), δ(H16–N15–C27)(12), δ(N15–C27—H16)(6)
16.	1471	1460	$\rho_s(CH_2)$	–CH_2–	δ(H23–C22–H24)(17), δ(H20–C19–H21)(13)
17.	1434	1439	ν(C=N), ν(C–N), ν(C=C)	imidazole	ν(C27–C29)(28), ν(C25–N15)(27), ν(C27–N15)(25), ν(C25–N14)(9)
18.	1346	1356	δ(COH), ν(C–N)	hydroxyl C–O–H, imidazole	δ(C17–O12–H13)(20), ν(C29–N14)(16), ν(C25–N14)(13), ν(C17–C18)(8)
19.	1327	1334	ν(skel), ν(C–N)	skeletal vib., imidazole	ν(C18–N14)(37), ν(C29–N14)(11), ν(C25–N15)(8), ν(C17–C18)(5)
20.	1272	1254	δ(COH), ν(skel)	hydroxyl C–O–H, skeletal vib.	δ(C17–O12–H13)(24), ν(C17–C18)(17), ν(C18–C19)(7), ν(C18–C22)(7)
21.	1221	1220	ν(C–N), $\rho_w(CH_2)$	imidazole, –CH_2–	ν(C25–N15)(17), ν(C29–N14)(9), δ(C18–C22–H23)(7), δ(C18–C19–H21)(6)
22.	1186	1174	δ(im)	imidazole	δ(N15–C25–H26)(49), δ(N14–C25–H26)(27), δ(H16–N15–C27)(7), δ(H16–N15–C25)(7)
23.	1156	1143	ν(P=O), δ(POH)	phosphonate P=O, P–O–H	ν(P1–O6)(46), δ(P1–O4–H5)(25), ν(P1–O3)(11)
24.	1141				δ(P2–O8–H9)(36), ν(P2–O7)(12), ν(C17–O12)(9)
25.	1109	1089	ν(C–O), δ(POH)	hydroxyl C–OH, phosphonate P–O–H	ν(C17–O12)(34), δ(P2–O8–H9)(16), δ(C18–C22–H23)(9)
26.	1090	1071	$\rho_w(CH_2)$	–CH_2–	δ(C18–C22–H24)(17), δ(C18–C22–H23)(15), δ(C19–C22–H24)(14), δ(C19–C22–H23)(13)
27.	1046	1049	ν(P=O), δ(POH)	phosphonate P=O, P–O–H	δ(P1–O4–H5)(52), ν(P1–O6)(16), ν(P2–O7)(16)
28.	1003	1006	δ_{ring}(im)	imidazole	δ(C27–C29–H30)(23), δ(N15–C25–H26)(20), δ(N14–C29–C27)(11), δ(N14–C25–N15)(7)

29.	987	976	ν(C–C), δ_{ring}(cycl)	–CH_2–CH_2–	ν(C18–C22)(13), ν(C18–C19)(11), δ(P2–C17–C18)(10), δ(C18–C19–C22)(7)
30.	979		$\rho_t(CH_2)$	–CH_2–	δ(C18–C22–H24)(21), δ(C18–C19–H20)(16), δ(C18–C19–H21)(14), δ(C18–C22–H23)(13)
31.	924	933	δ_{ring}(im)	imidazole	δ(C25–N15–C27)(28), δ(N14–C29–C27)(19), δ(N14–C25–N15)(18), δ(N15–C27–C29)(14)
32.	918	906	ν(P–O), δ_{ring}(im)	phosphonate P–O, imidazole	ν(P1–O3)(24), δ(N14–C25–N15)(15), δ(C25–N15–C27)(9), ν(P1–O6)(8)
33.	836	831	ν(P–O)	phosphonate P–OH	ν(P2–O10)(41), ν(P2–O8)(21)
34.	824		ν(P–C)	phosphonate P–C	ν(P2–C17)(16), ν(P1–C17)(14), δ(P2–C17–C18)(10), ν(P2–O10)(7)
35.	808	796	$\rho_r(CH_2)$	–CH_2–	δ(H20–C19–C22)(31), δ(H21–C19–C22)(28), δ(C19–C22–H24)(26), δ(C19–C22–H23)(24)
36.	750	758	ν(P–O)	phosphonate P–OH	ν(P2–O8)(33), ν(P1–O4)(17), ν(P2–O10)(5)
37.	715	710			ν(P1–O4)(45), ν(P2–O8)(7)
38.	663	684	τ(im)	imidazole	τ(N14–C25–N15–C27)(28), τ(C17–C18–N14–C25)(17), τ(N14–C29–C27–N15)(11)
39.	636	646			τ(N14–C29–C27–N15)(64), τ(C29–C27–N15–C25)(11), τ(N14–C25–N15–C27)(4)
40.	601	595			τ(N14–C25–N15–C27)(49), τ(N14–C29–C27–N15)(26), τ(C29–C27–N15–C25)(16)
41.	573	575	δ(COH)	hydroxyl C–O–H	δ(C17–O12–H13)(53)
42.	545	533	τ(skel), δ(skel)	skeletal vib.	τ(N14–C18–C17–P1)(17), δ(C18–N14–C29)(11), δ(P2–C17–C18)(7), δ(C18–N14–C25)(5)
43.	526	513			δ(C18–N14–C25)(12), τ(N14–C18–C17–P1)(9), δ(C18–N14–C29)(8), ν(C17–P2)(7)
44.	487	462	δ(OPO), δ(skel)	phosphonate O–P–O skeletal vib.	δ(O6–P1–C17)(14), δ(P1–C17–C18)(9), δ(C18–N14–C25)(5), δ(O3–P1–O4)(5)
45.	456	433			δ(O7–P2–C17)(6), δ(O7–P2–O10)(6), δ(C18–N14–C29)(6)
46.	396	405			δ(O3–P1–O6)(22), δ(O12–C17–C18)(12), δ(C18–N14–C25)(7), δ(O3–P1–O4)(5)

[a]Scaling factors for the calculated harmonic frequencies: 0.946 for modes 1-13, 0.973 for modes 14-20, 1.000 for modes 21-46. [b]Abbreviations: br – broad, ν – stretching, δ – in-plane bending, ρ_s – scissoring, ρ_w – wagging, ρ_t – twisting, ρ_r – rocking, τ – torsion. Subscripts: as – antisymmetric; s – symmetric. [c]Vibrational bands assignment for the most characteristic functional groups based on the significant contribution in the potential energy distribution.[d]The PED values are listed if a contributor is among the top four and is ≥ 4%.

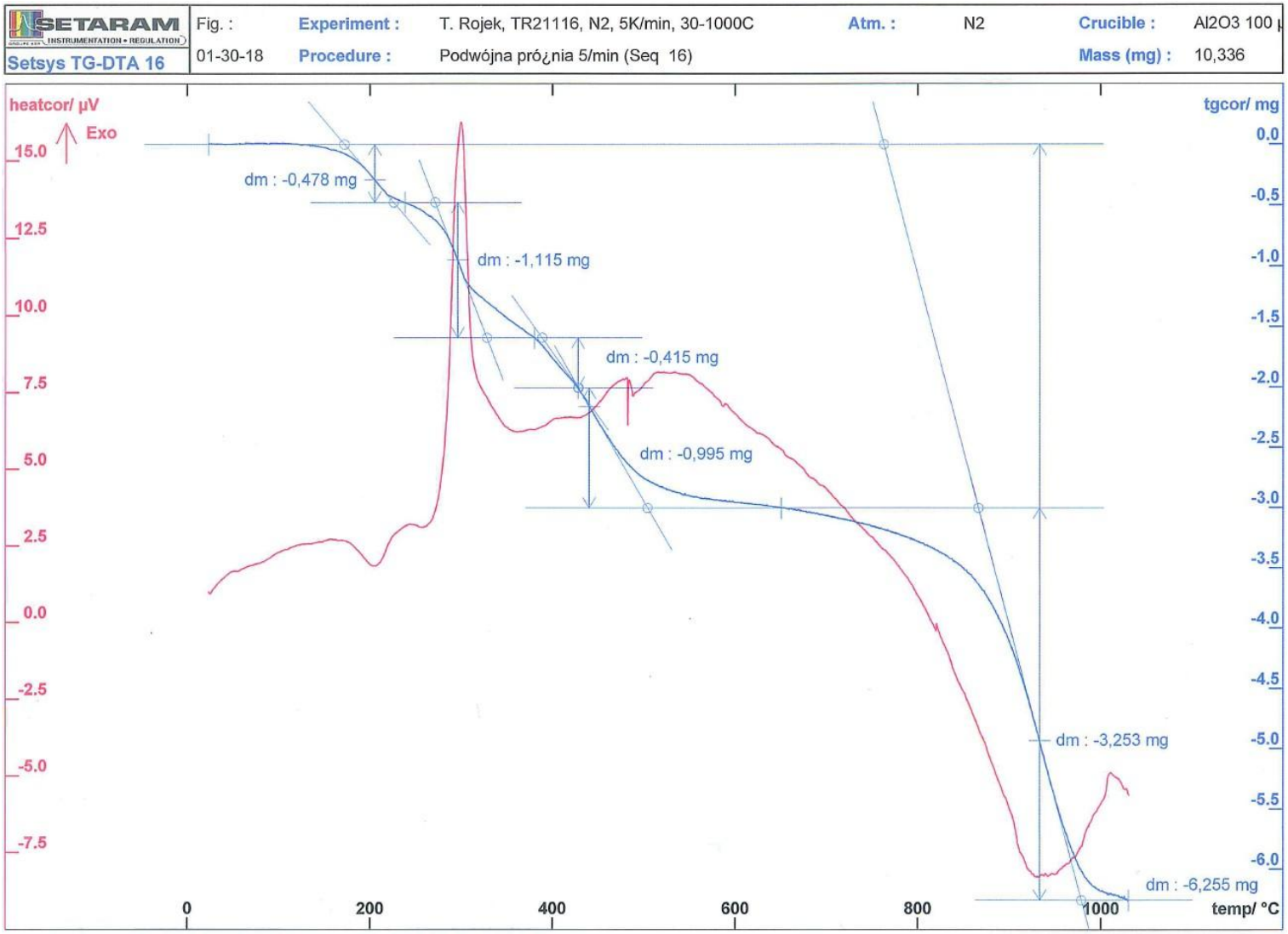

Figure S18. TG-DTA plot for the $Co(H_2cppZol)(H_2O)\cdot 2H_2O$ complex (**1a**).

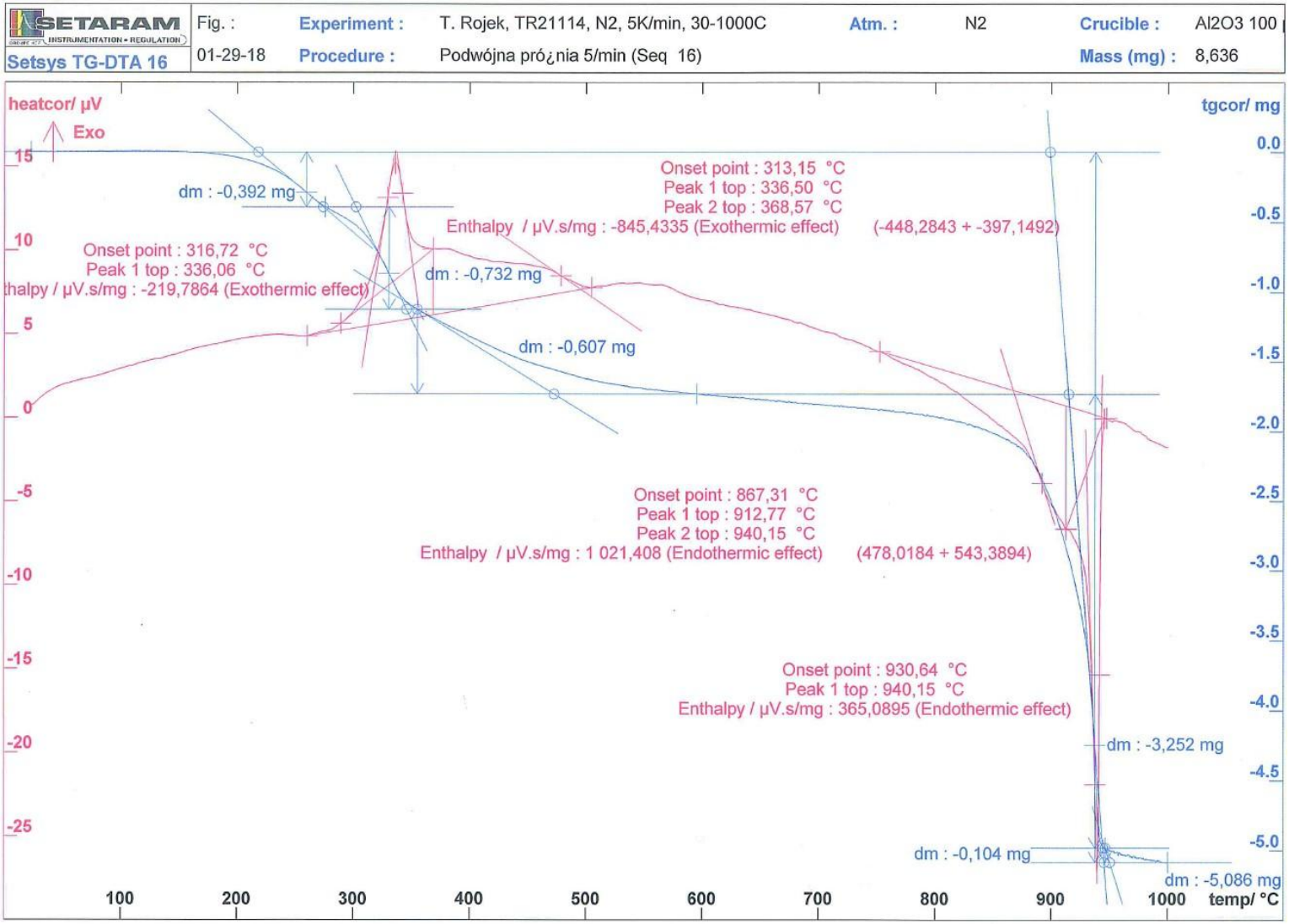

Figure S19. TG-DTA plot for the Ni(H_2cppZol)(H_2O)·2H_2O complex (**1b**).

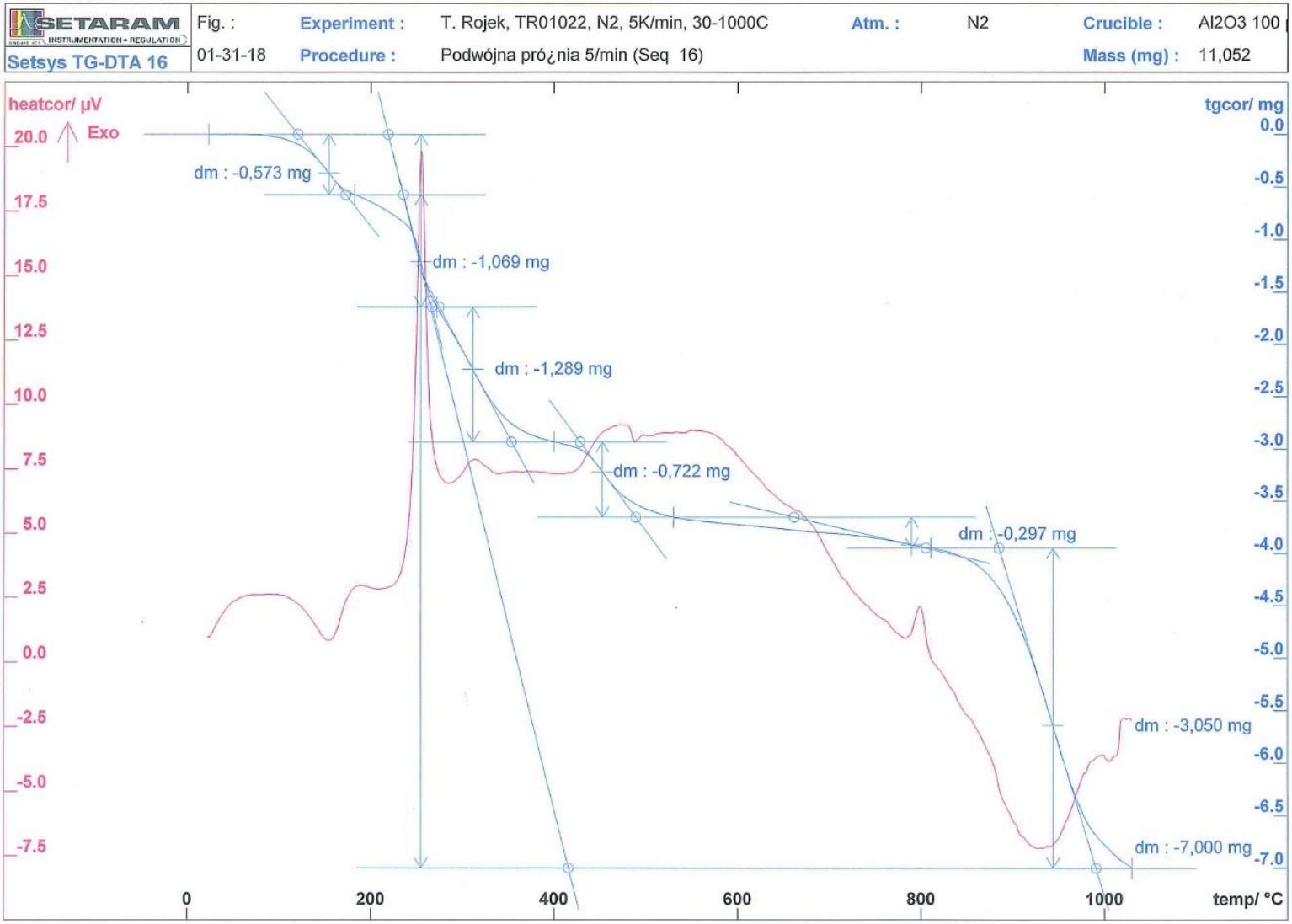

Figure S20. TG-DTA plot for the $Co(H_2cbtZol)(H_2O)\cdot 2H_2O$ complex (**2a**).

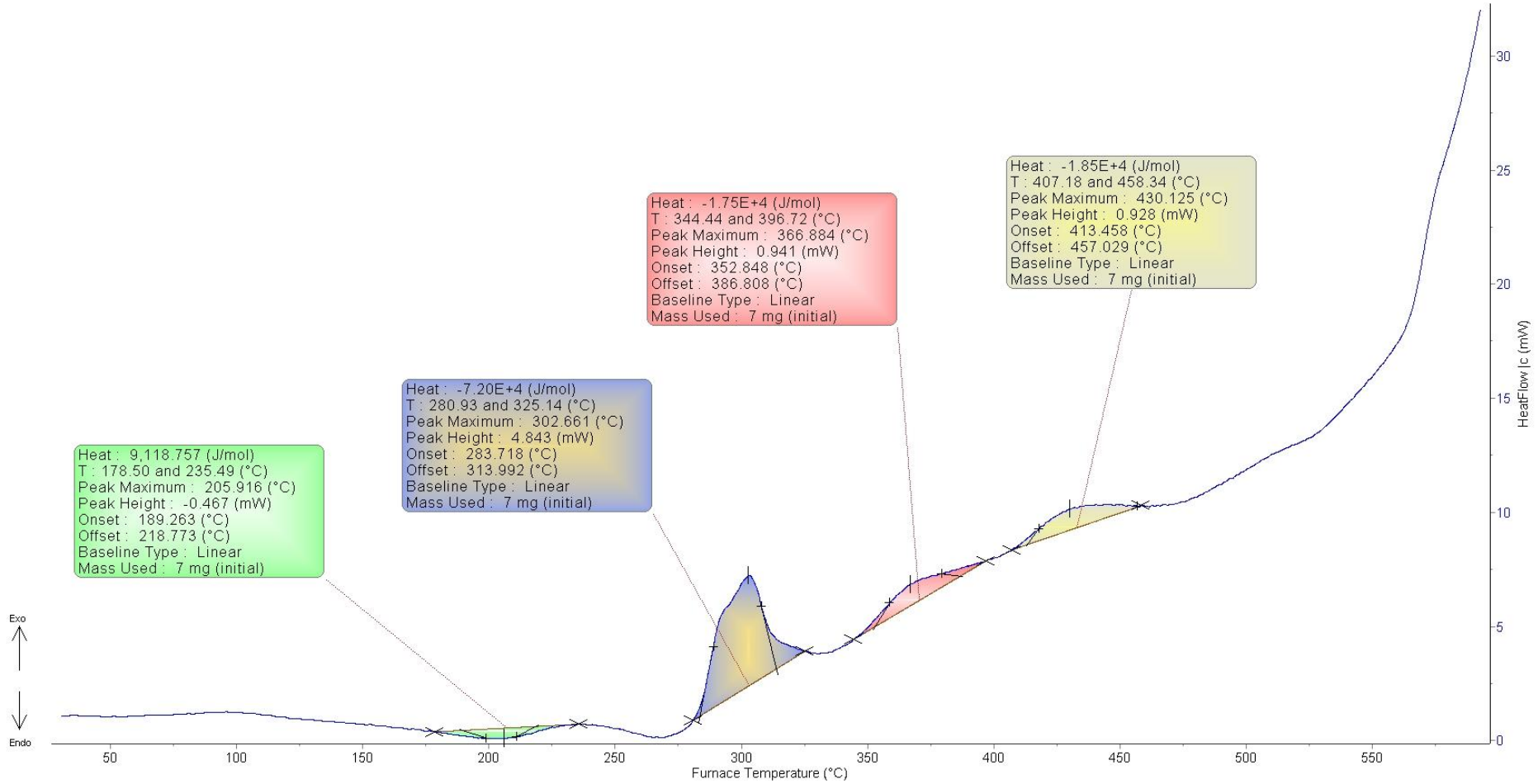

Figure S21. DSC plot for the $Co(H_2cppZol)(H_2O)\cdot 2H_2O$ complex (**1a**).

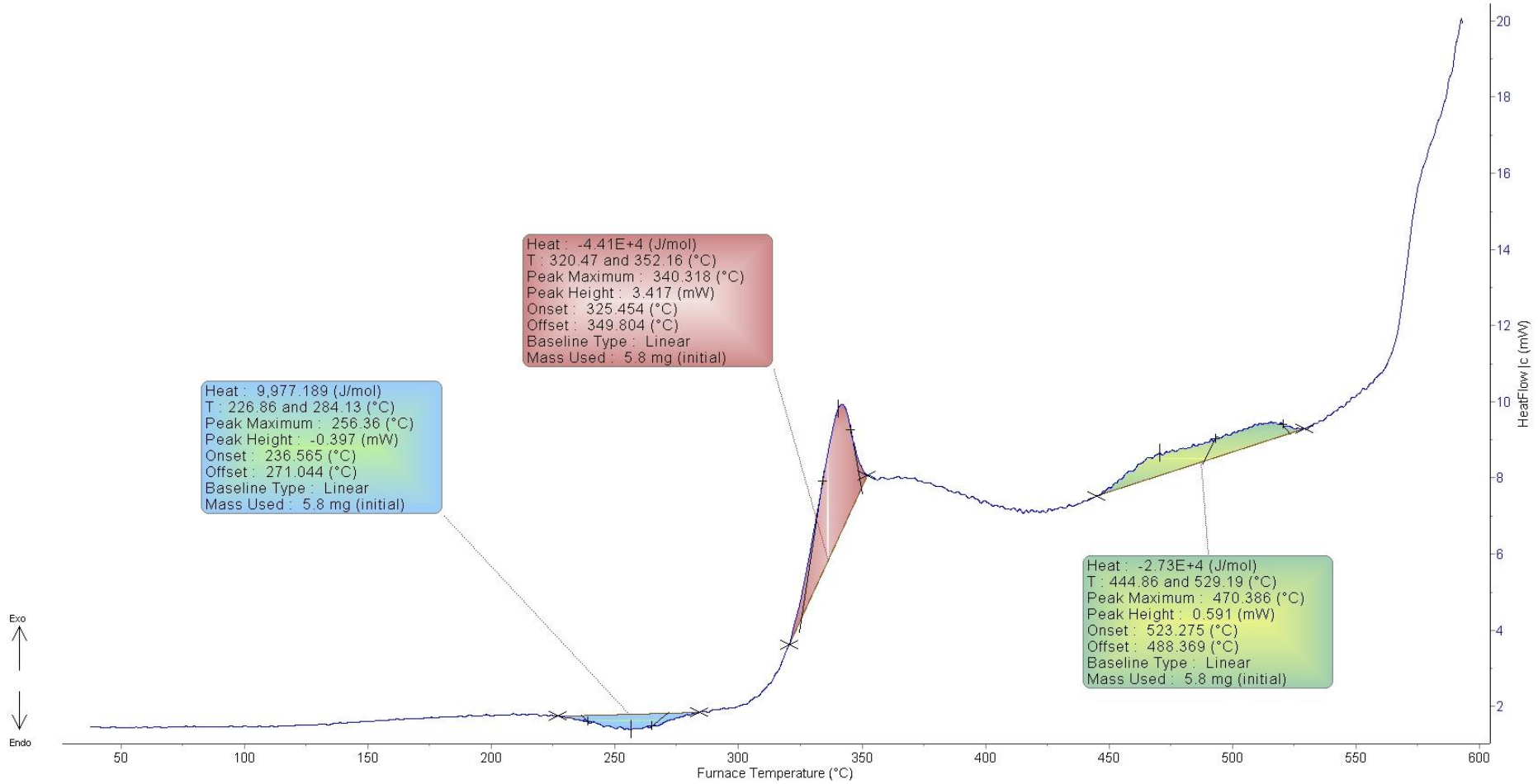

Figure S22. DSC plot for the Ni(H_2cppZol)(H_2O)·2H_2O complex (**1b**).

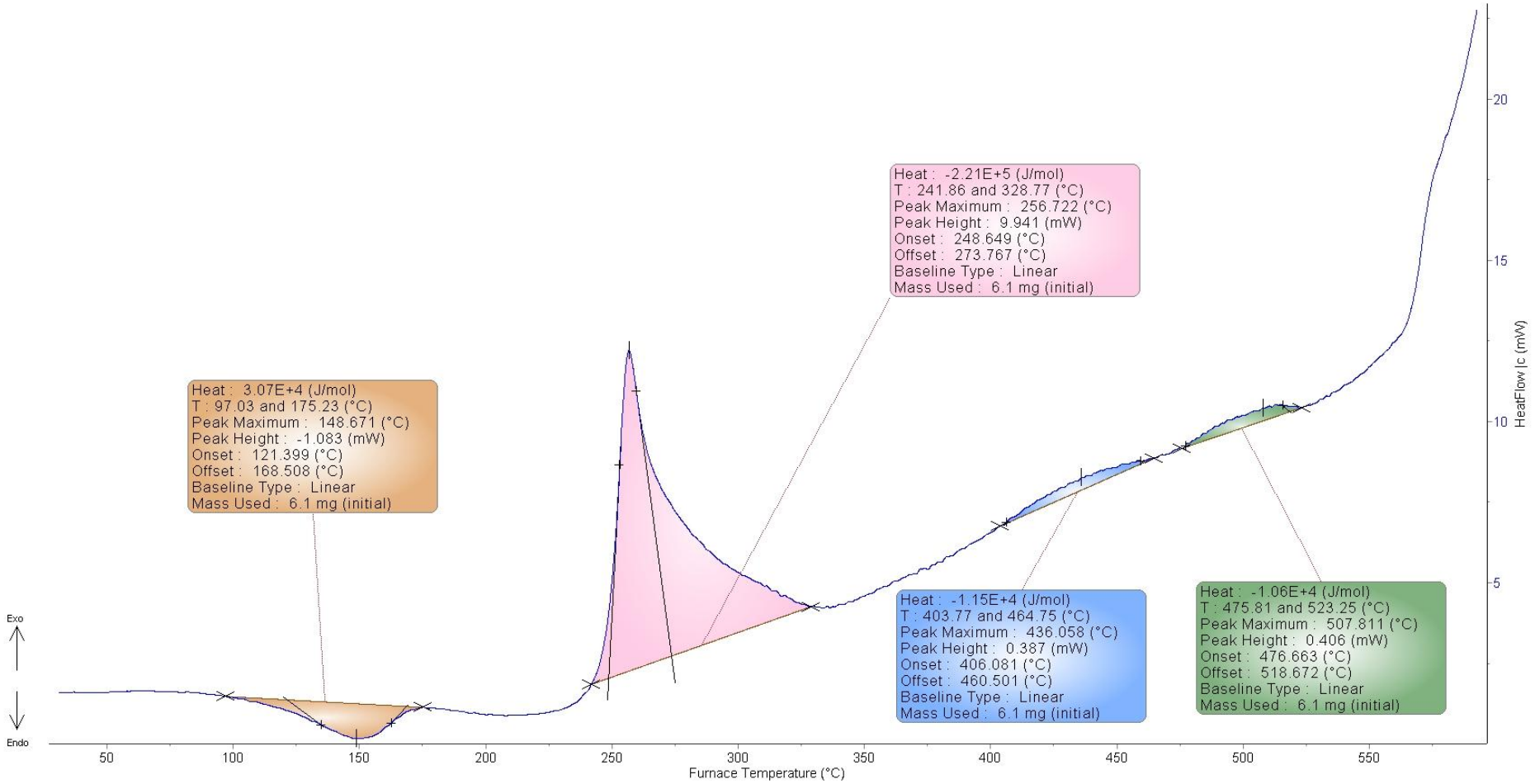

Figure S23. DSC plot for the $Co(H_2cbtZol)(H_2O)\cdot 2H_2O$ complex (**2a**).

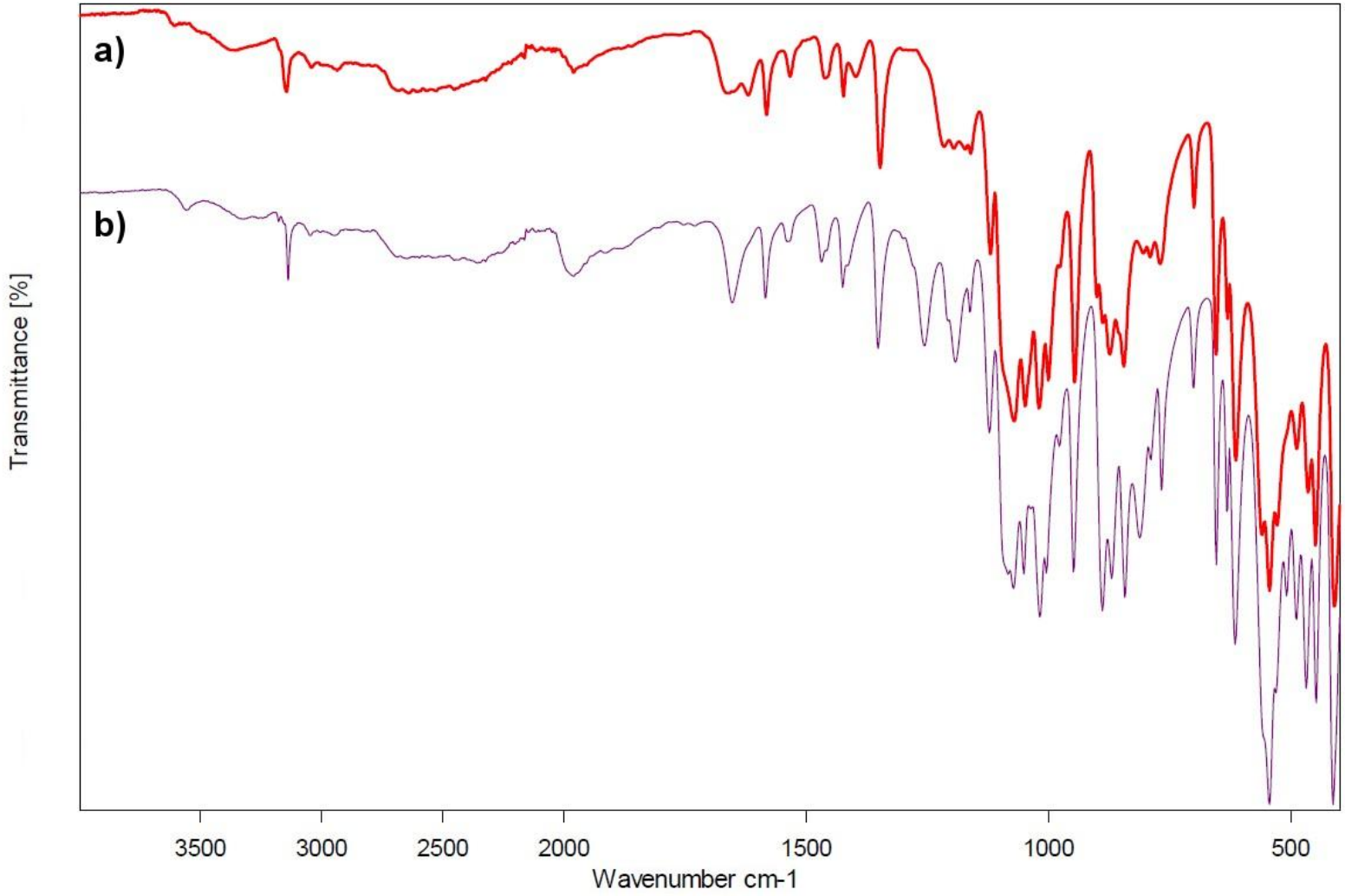

Figure S24. IR spectra of (a) crystalline **1a** and solid obtained by heating sample of the complex up to (b) 219 °C.

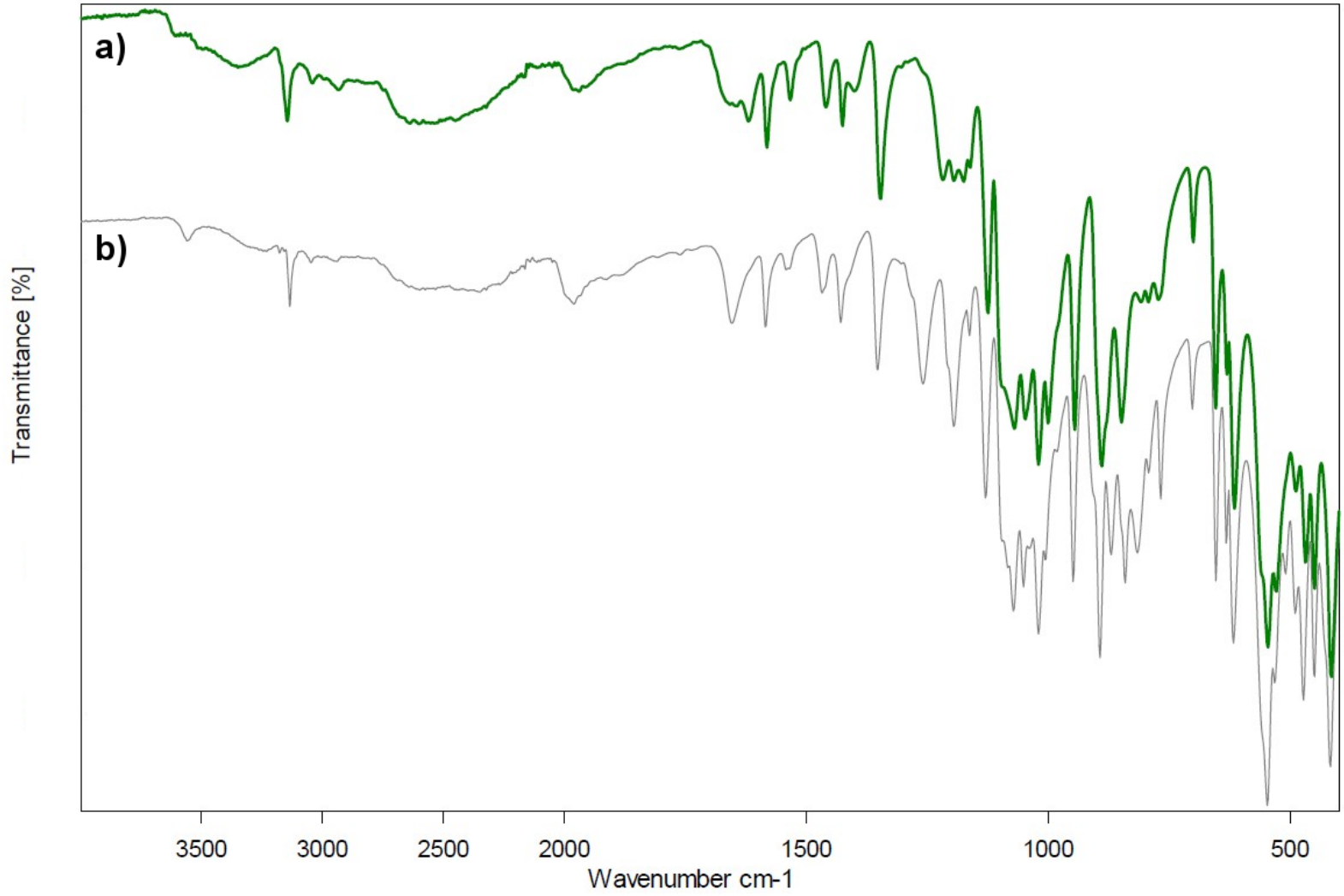

Figure S25. IR spectra of (a) crystalline **1b** and solid obtained by heating sample of the complex up to (b) 284 °C.

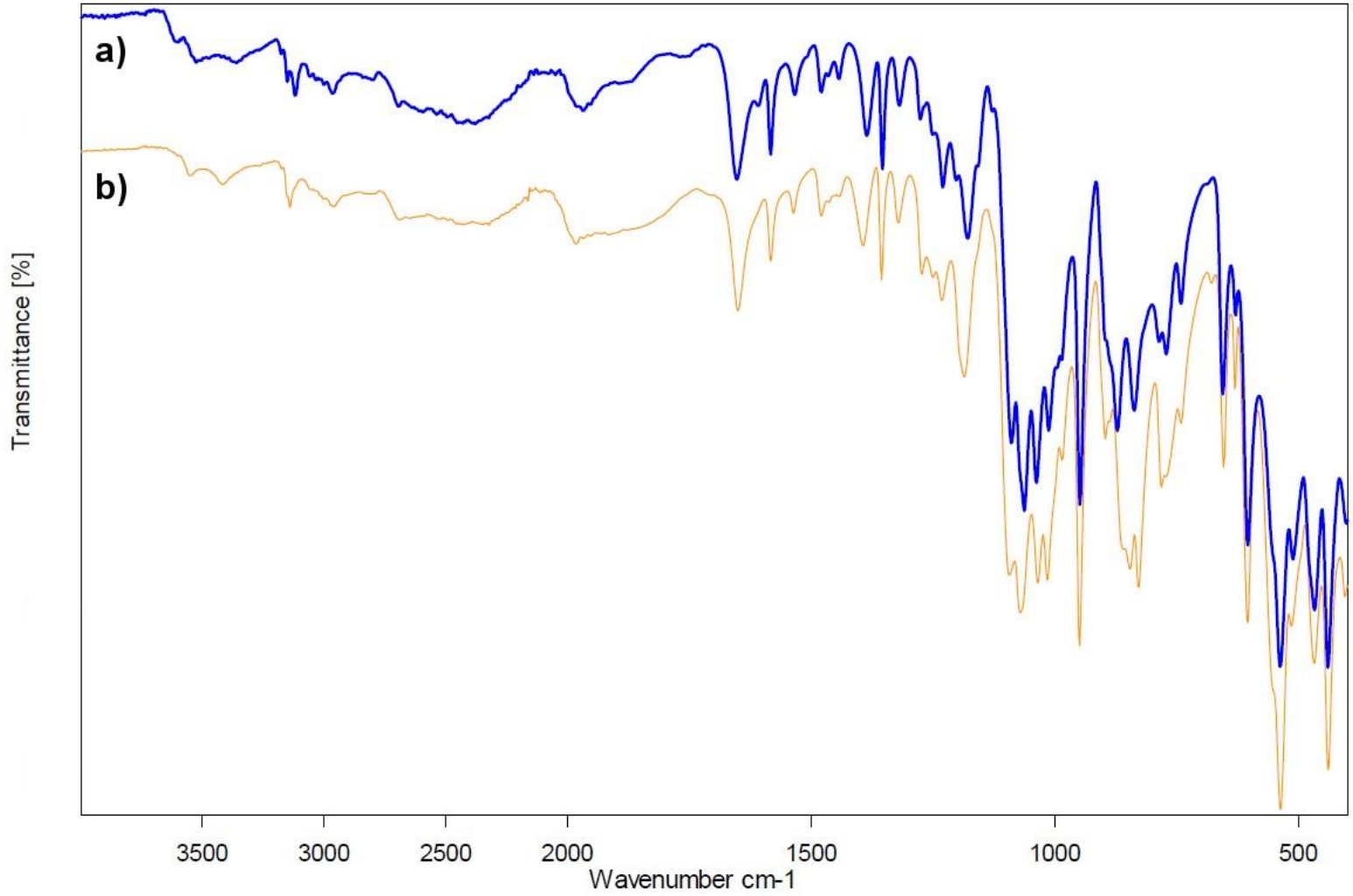

Figure S26. IR spectra of (a) crystalline **2a** and solid obtained by heating sample of the complex up to (b) 175 °C.

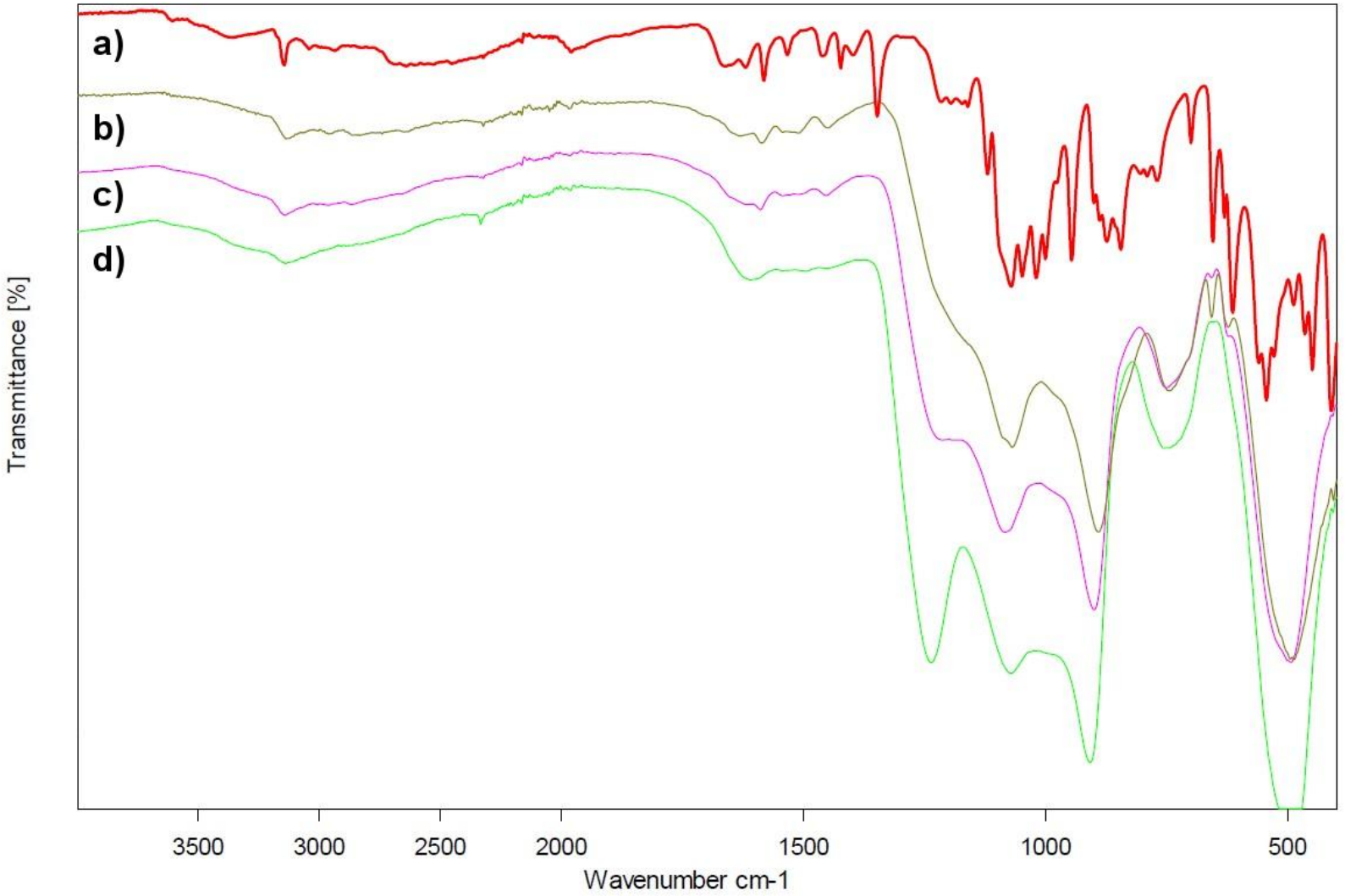

Figure S27. IR spectra of (a) crystalline **1a** and solids obtained by heating sample of the complex up to (b) 314 °C; (c) 387 °C; (d) 457 °C.

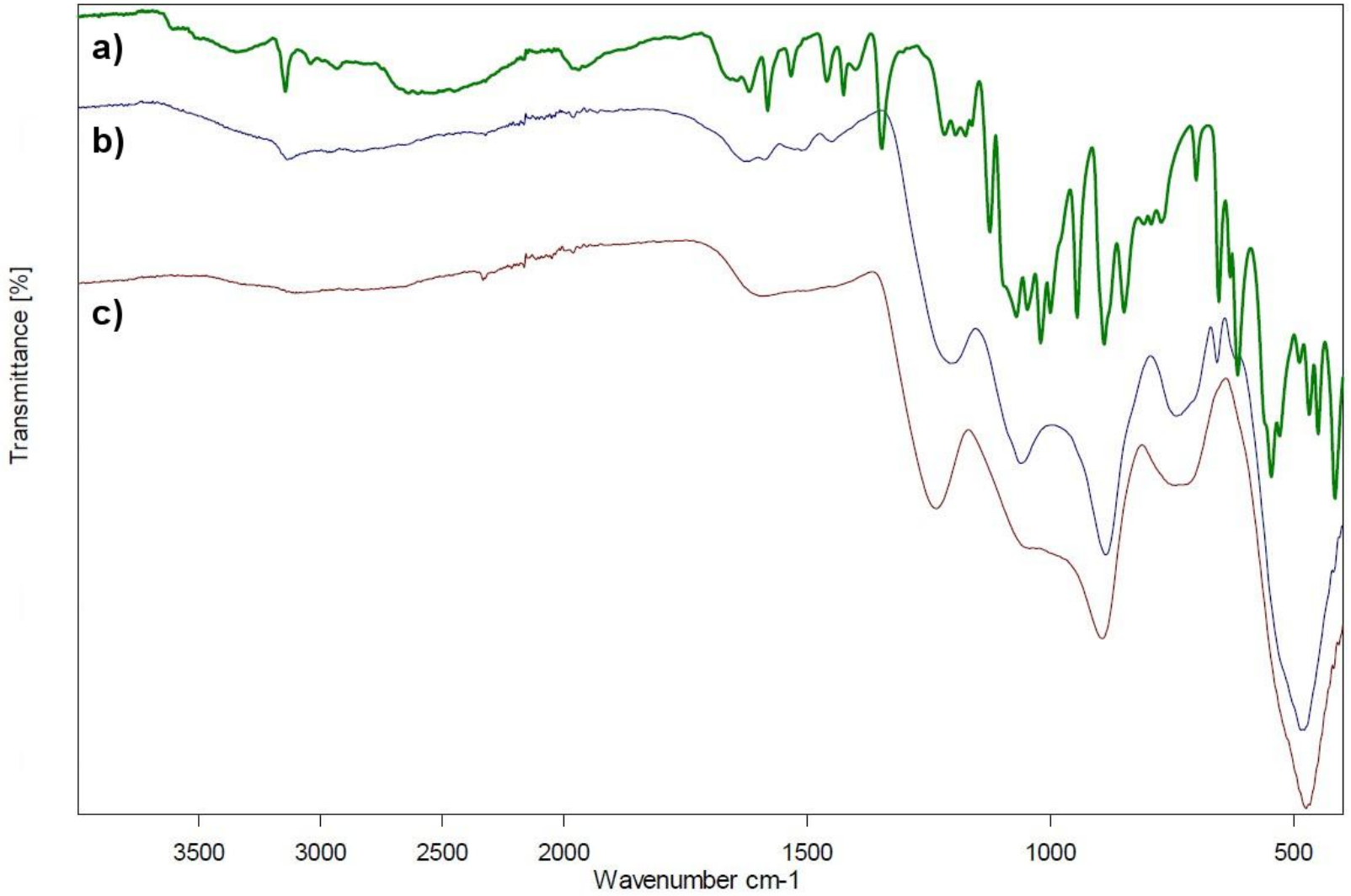

Figure S28. IR spectra of (a) crystalline **1b** and solids obtained by heating sample of the complex up to (b) 352 °C, (c) 529 °C.

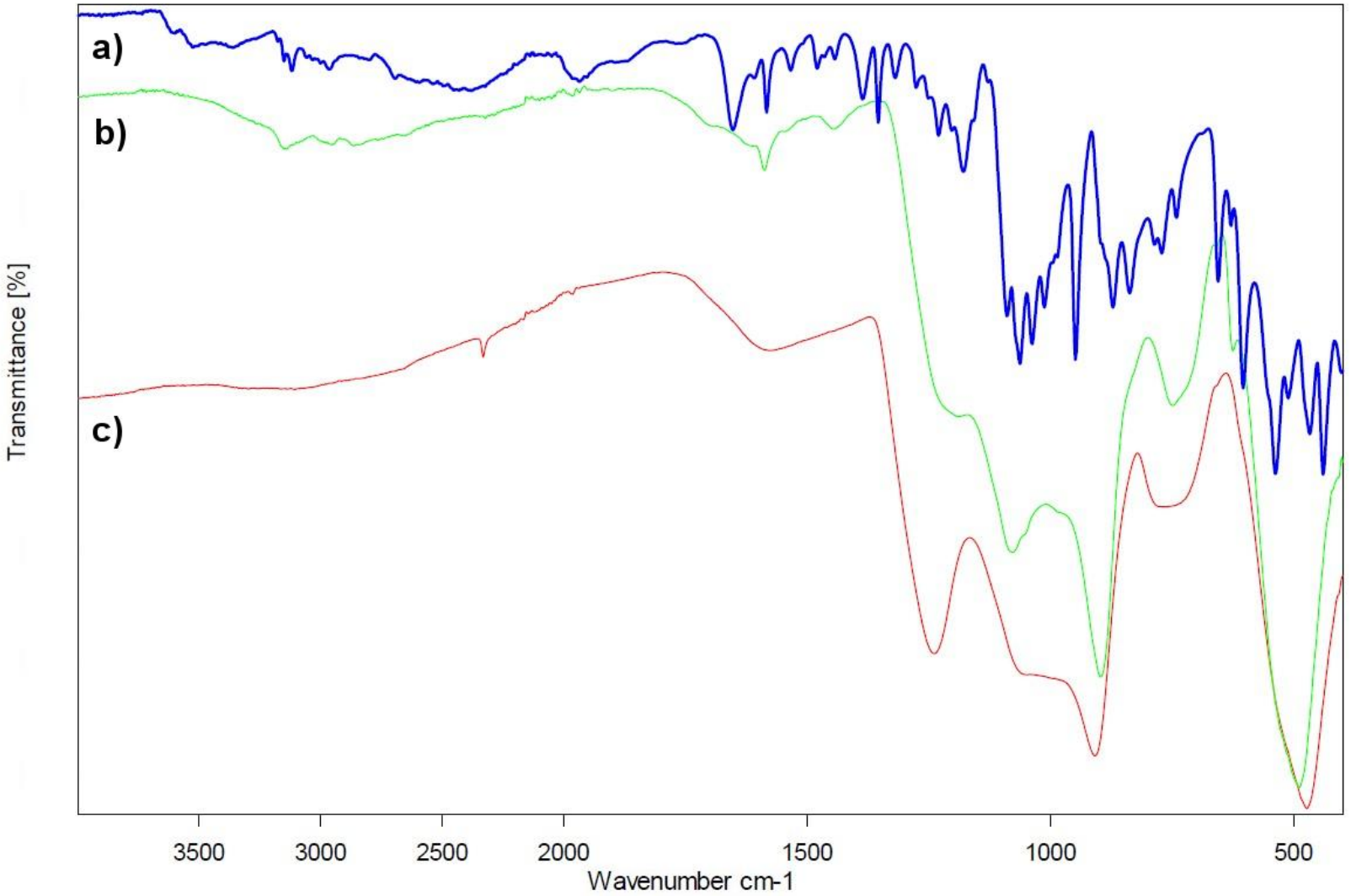

Figure S29. IR spectra of (a) crystalline **2a** and solids obtained by heating sample of the complex up to (b) 329 °C, (c) 525 °C.

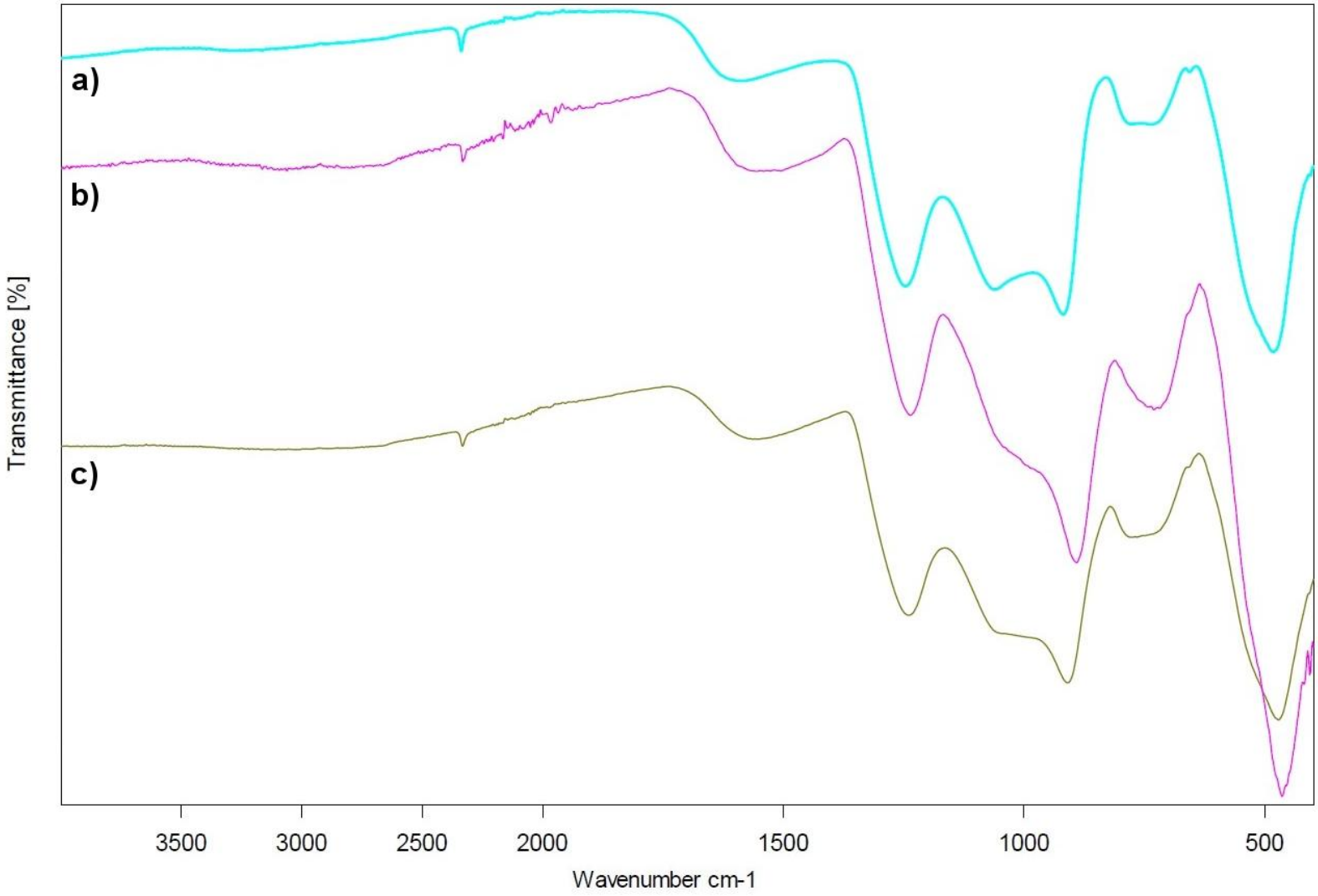

Figure S30. A comparison of IR spectra of solid residues, obtained by heating crystalline samples of (a) **1a**, (b) **1b** and (c) **2a** up to 600 °C.

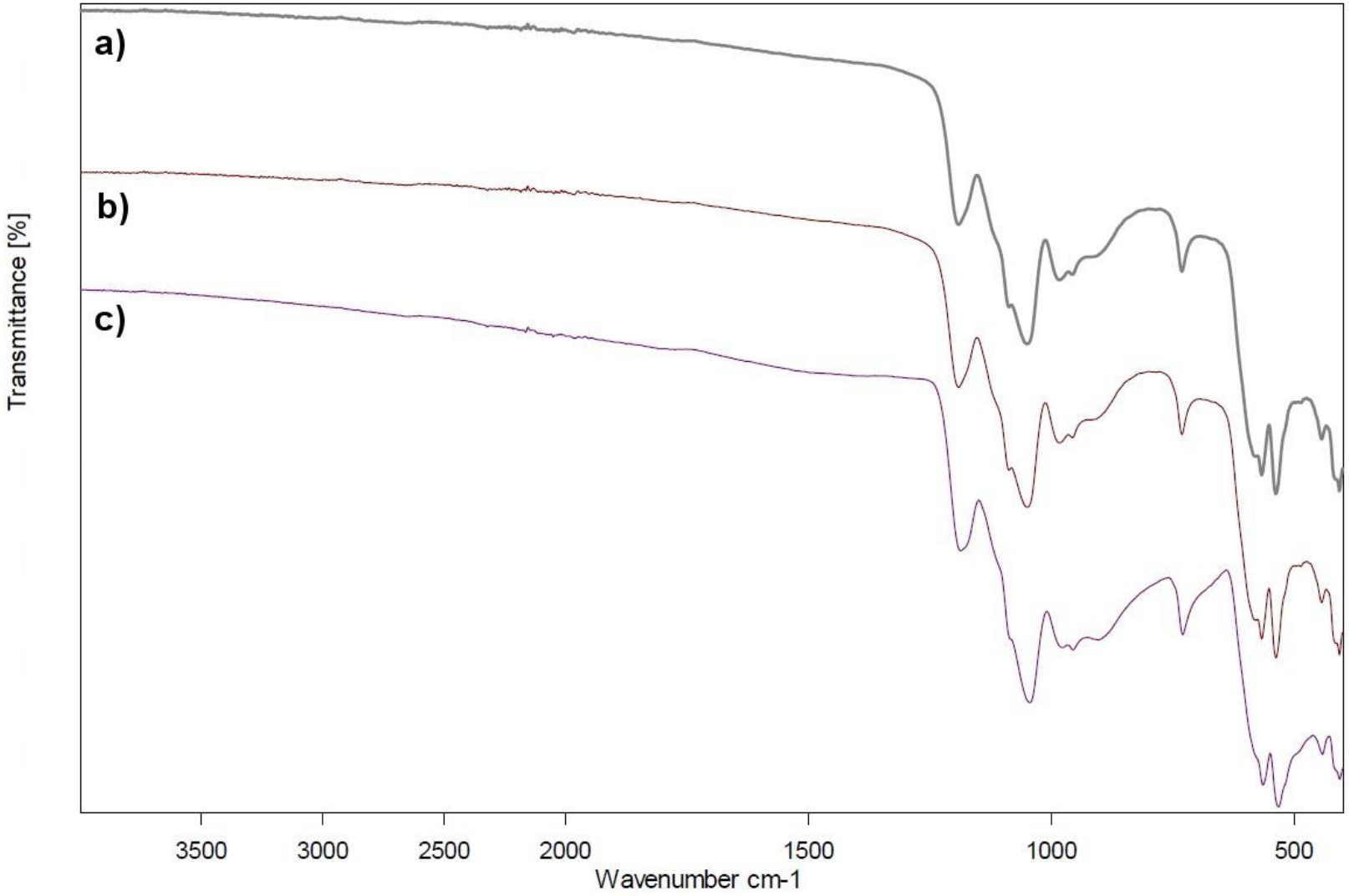

Figure S31. A comparison of IR spectra of solid residues, obtained by heating crystalline samples of (a) **1a**, (b) **1b** and (c) **2a** up to 1000 °C.

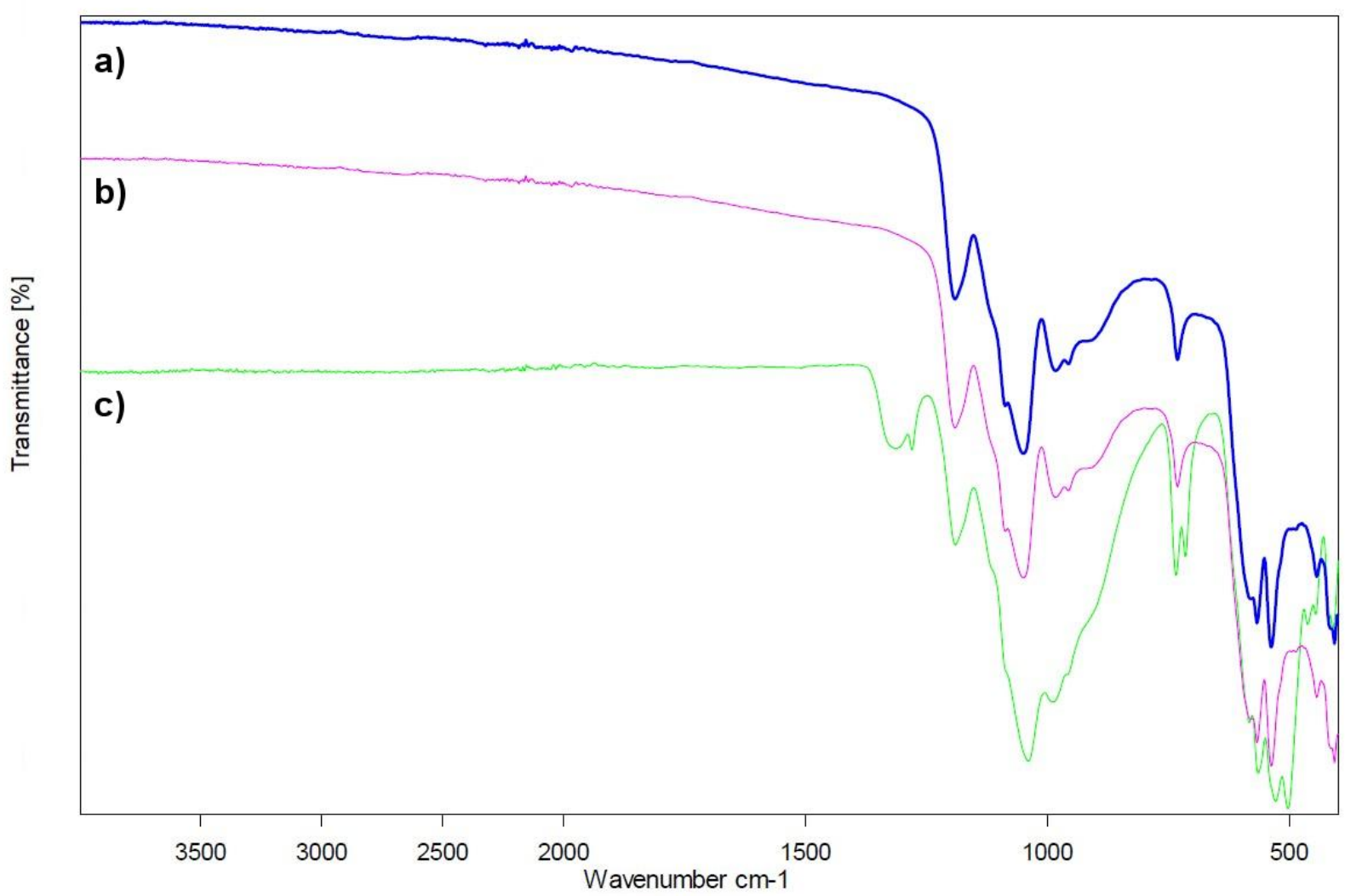

Figure S32. A comparison of IR spectra of solid residues, obtained by heating crystalline samples of (a) **1a**, (b) **1b** and (c) Co(II) complex of cyclopropane substituted analog of zoledronic acid – $Co_3(HcppZol)_2(H_2O)_6 \cdot 6H_2O$ up to 1000 °C.

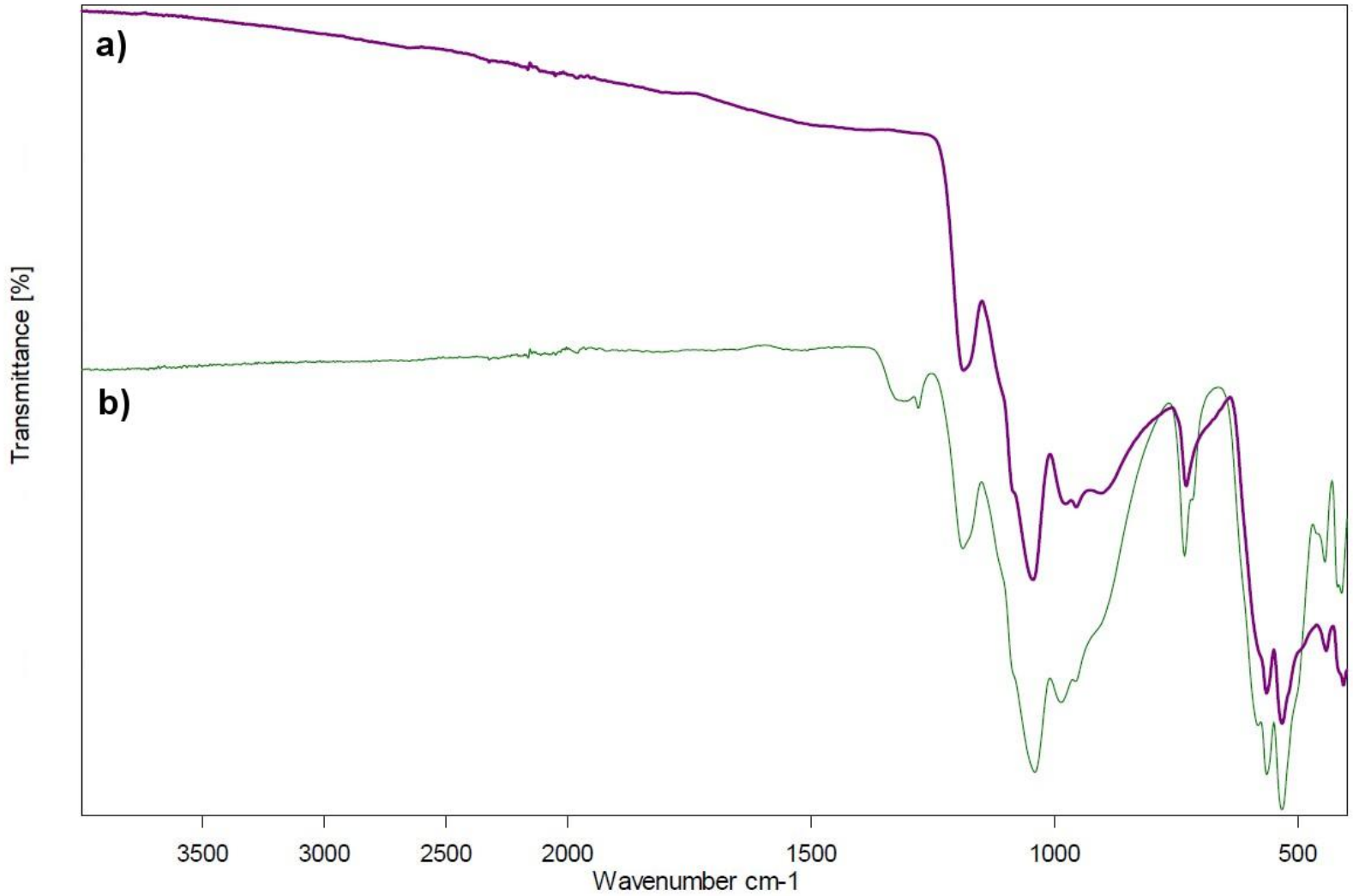

Figure S33. A comparison of IR spectra of solid residues, obtained by heating a crystalline sample of (a) **2a** and (b) Co(II) complex of cyclobutane substituted analog of zoledronic acid – $Co_3(HcbtZol)_2(H_2O)_6 \cdot 6H_2O$ up to 1000 °C.

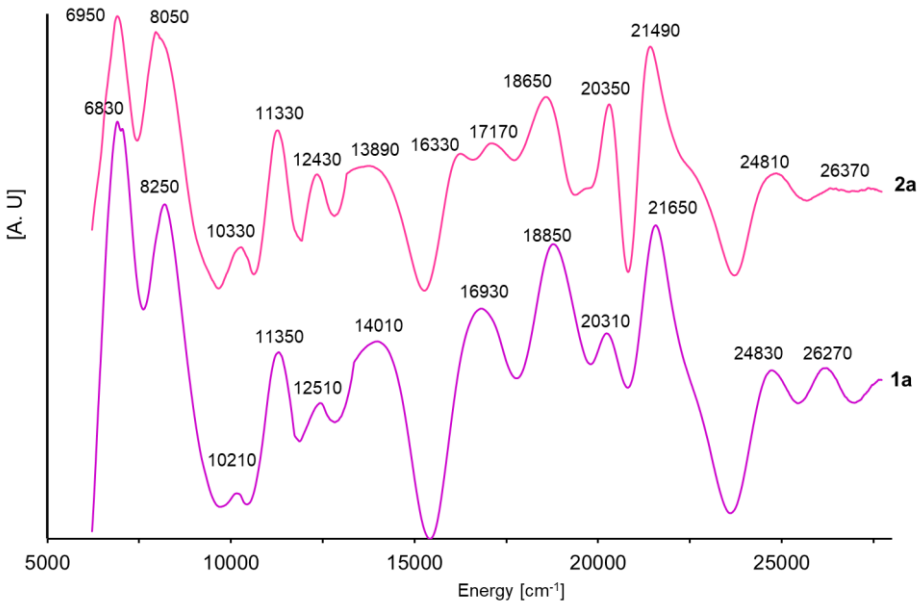

Figure S34. The effect of filtering process of *d-d* bands for the spectra of cobalt(II) complexes (**1a**, **2a**) in the 5000-28000 cm^{-1} spectral range (spectral range parameters: step = 20 cm^{-1}, α = 400 and N = 40 (**1a**), step = 20 cm^{-1}, α = 400 and N = 30 (**2a**)).

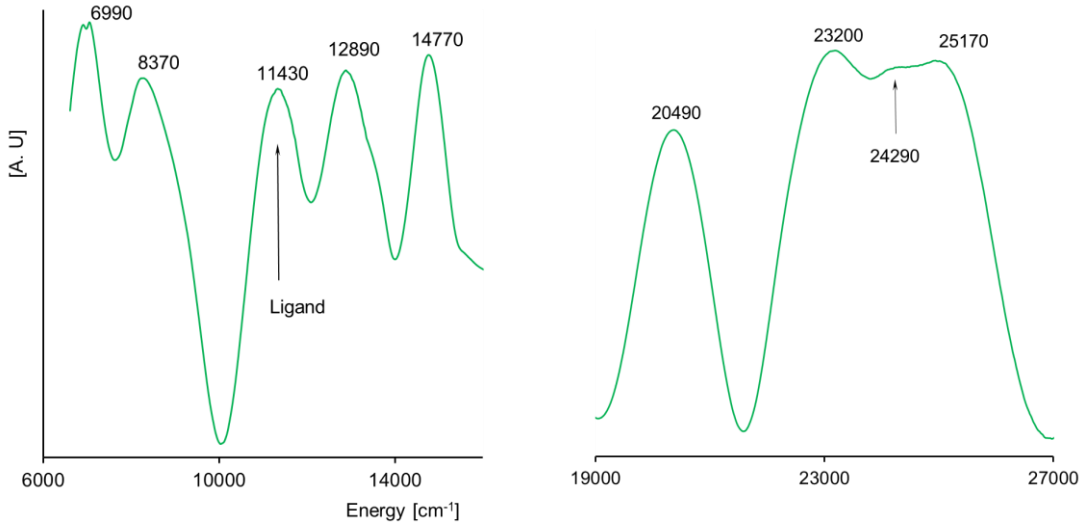

Figure S35. The effect of filtering process of *d-d* bands for the spectrum of the nickel(II) complex (**1b**) in the 6000-27000 cm^{-1} spectral range (spectral range parameters: step = 20 cm^{-1}, α = 500, N= 40).

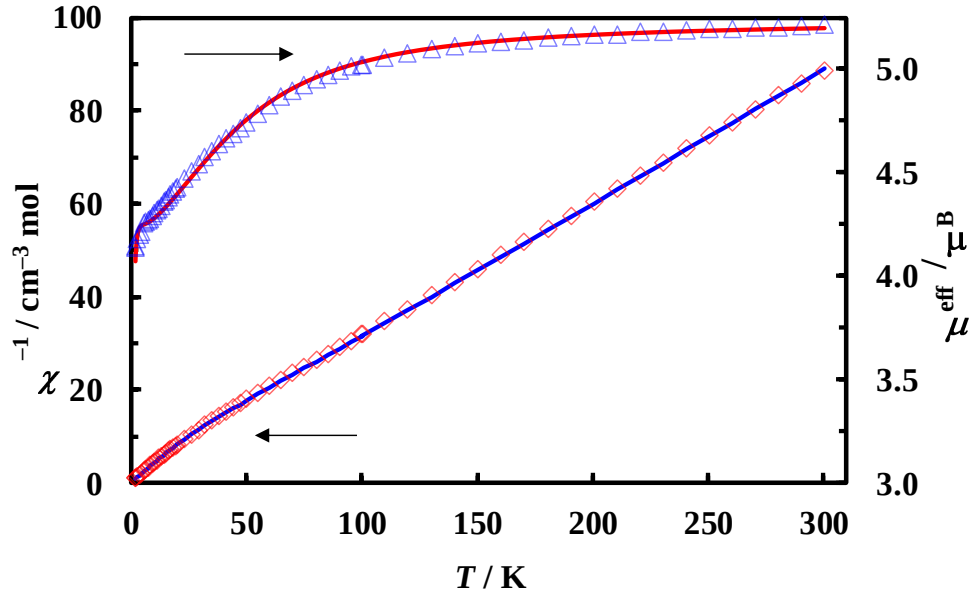

Figure S36. Variation of χ^{-1} (diamonds) and μ_{eff} (triangles) for **1a** with temperature. The lines represent the fit to the alternating-exchange spin-chain model (see the main text).

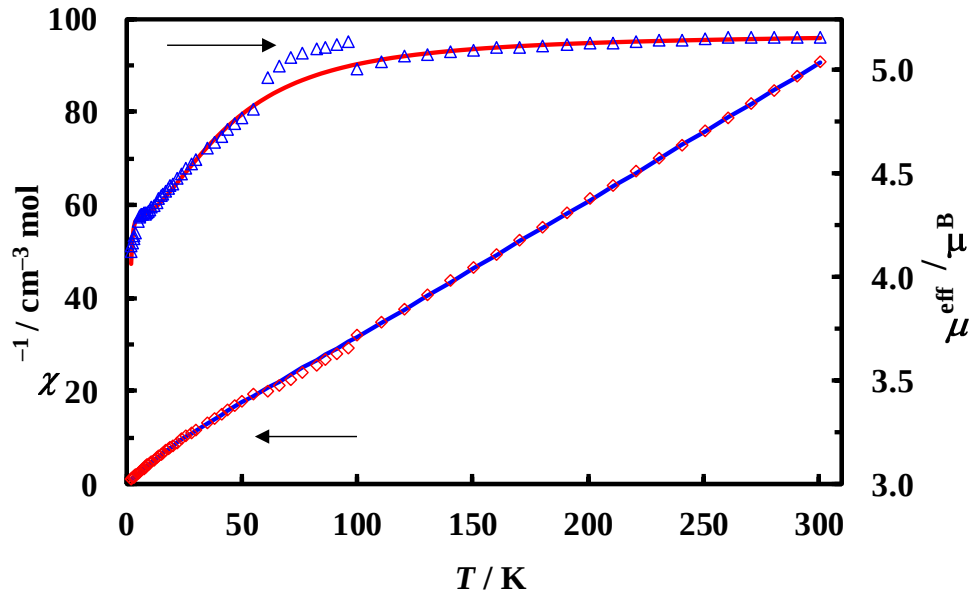

Figure S37. Variation of χ^{-1} (diamonds) and μ_{eff} (triangles) for **2a** with temperature. The lines represent the fit to the alternating-exchange spin-chain model (see the main text).

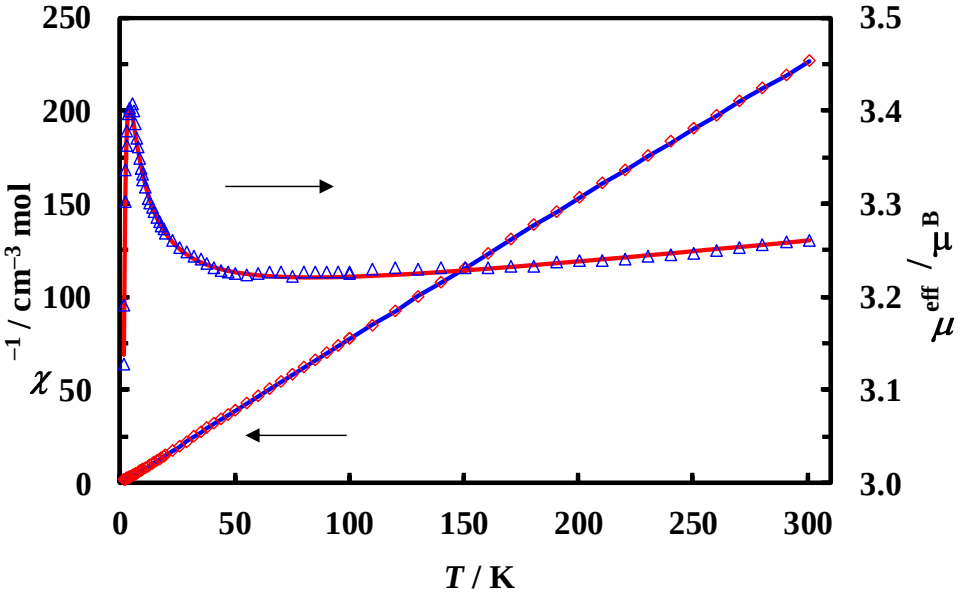

Figure S38. Variation of χ^{-1} (diamonds) and μ_{eff} (triangles) for **1b** with temperature. The lines represent the fit to the alternating-exchange spin-chain model (see the main text).

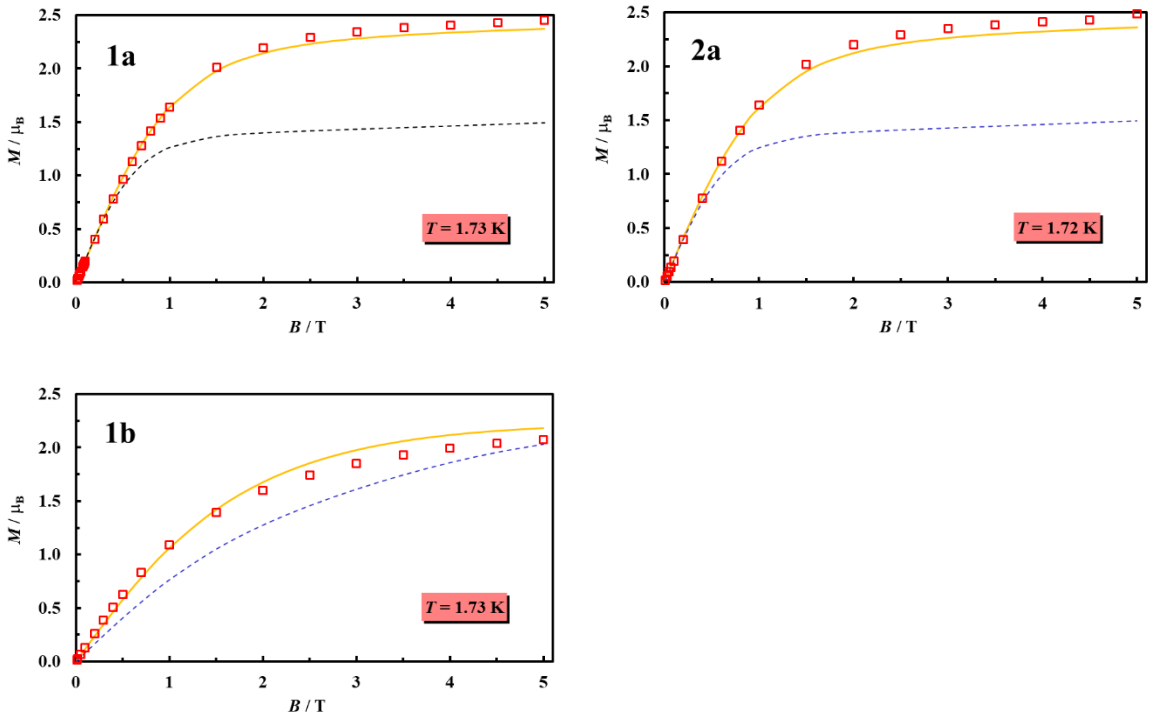

Figure S39. Magnetization curves versus applied magnetic field. The solid lines were calculated using parameters *g*, *D*, *TIP* identical to those obtained for magnetic susceptibility, but without magnetic exchange. The dotted lines for cobalt compounds (**1a** and **2a**) are calculated with changed signs of the *D* parameters. For **1b,** the best fit parameters for $D > 0$ (D = +5.0 cm^{-1}, g_{av} = 2.25, *TIP* = 191·10^{-6}emu/Ni).

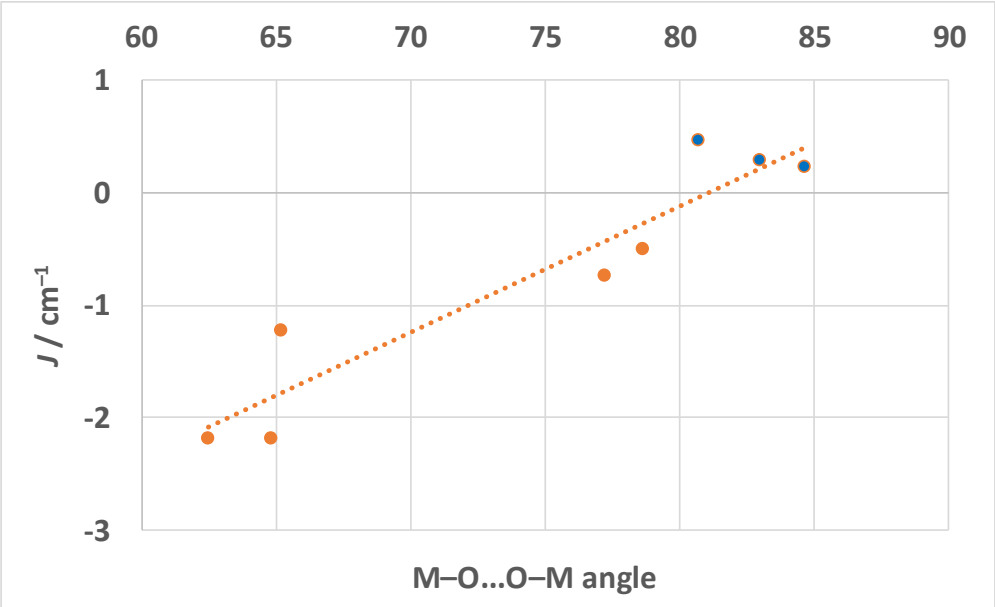

Figure S40. Magnetic coupling constants for Co(II) complexes as a function of the Co–O···O–Co torsion angle over the O–P–O bridge.

Table S7. Selected geometric parameters of the −O−P−O− bridges together with the corresponding magnetic exchange constants

			P1				**P2**	
Compound	***d* / Å**	***Torsion angle***		***J*$_1$ / cm^{-1}**	***d* / Å**	***Torsion angle***	***J*$_2$ / cm^{-1}**
	Co-Co	**CoO1···O2Co**			**Co-Co**	**CoO4···O6Co**	
1a	4.815	78.66		-0.50	4.820	84.65	0.23
2a	4.820	77.26		-0.74	4.822	82.99	0.29

Compounds $Co_3(HL)_2(H_2O)_6{\cdot}6H_2O$

HL	***d* / Å**	***Torsion angle***	***d* / Å**	***Torsion angle***	***J*$_1$ / cm^{-1}**	***d* / Å**	***Torsion angle***	**Θ / K**
-	**Co1-Co2**	**Co1O2···O3Co2**	**Co1···Co2**	**Co1O5···O6Co2**		**Co2-Co2**	**Co2O4···O6Co2**	
			average					
HcbtZol^{3} [ref. 13]	5.012	77.41 52.96		65.19	-1.23	4.804	82.56	+0.26 K
HdmtZol^{3-} [ref. 12]	4.961	74.07 50.96		62.52	-2.19	4.719	83.32	+0.13 K
HcppZol^{3-}	5.035	78.62 51.00		64.81	-2.19	4.771	81.02	+0.40 K